Chapter 6

SIGNAL PROCESSING FOR IMPROVED DETECTIVITY

- ***How can compensation or correction be used to improve detectivity?***
- ***How can feedback be applied to reduce an error by source loading?***
- ***What is the difference between filtering and coherent detection?***
- ***How should a lock-in amplifier be used?***
- ***When can correlation be used to improve detectivity?***
- ***How can digital signal processing be used to improve detectivity?***

6.1 Introduction

In the preceding chapters the effects of several sources of uncertainty on the detection limit has been analysed. The effect of the different sources of uncertainty in a system are expressed in terms of equivalent input sources which should in principle be smaller than the input signal, to ensure that the signal intended can be measured.

The input signal intended is in principle below the detection limit (i.e. not measurable) if the input-referred equivalent sources of uncertainty (error) result in an input signal that is larger than this signal to be measured (also considering the inaccuracy specification).

If noise is the dominating source of uncertainty, then the detection limit is the signal power that is determined by the noise spectral power of the equivalent input noise sources over the measurement bandwidth, with the specified SNR.

The measurand is not measurable if the input signal power is below the detection limit. However, this simple conclusion (i.e. 'sorry, we cannot help you') is unacceptable if the problem at hand has a huge impact on society. In the case of such a demanding measurement problem, an analysis is usually requested of instrumentation techniques that may be applicable to make the signal measurable. Three different approaches are possible:

- Reduce the effect of the unfavourable system property or interfering signal
- Make use of prior knowledge on an essential property of the signal
- Apply signal processing to enhance the SNR

These techniques are discussed in this chapter.

As is discussed in Chapter 5, EMI can be reduced using shielding. Moreover, **compensation** and **correction** techniques are available at the system level to reduce undesirable cross-sensitivities. These techniques are discussed in Section 6.2. **Feedback** can be used to reduce undesirable system properties through design, such as increasing the input impedance of an instrument for Voltage read-out in order to reduce loading of the measurand by the measurement, and is discussed in Section 6.3.

Prior knowledge of the essential properties of the measured signal can be used to enable the instrument to selectively measure only the desired input signal, thus effectively reducing the susceptibility of the measurement to noise. There are two special signal features of interest:

- The frequency spectrum of the measurement signal versus that of the interfering signal
- The timing of information in a triggered event

The first special case is based on prior knowledge about the frequency spectrum. As is discussed in Section 2.4.3, filtering can be applied to improve the signal-to-noise ratio by the selective attenuation of the out-of-band noise components. Frequency filtering is highly effective for improving the SNR in the case a relatively narrowband input signal is contained within wideband noise (e.g. a Wheatstone bridge output with white noise). Alternatively, filtering is used in case of a wideband input signal with a spectrally well-defined, narrowband noise component of high amplitude (e.g. capacitively coupled mains voltage at 50 Hz). In this case, the purpose of filtering is to selectively attenuate the in-band noise component with minimum loss of the signal content.

Filtering is particularly powerful in combination with modulation techniques, which can be applied in e.g. the AC-operated Wheatstone bridge. The implementation of filtering without the practical problems of high-Q band-pass filters, is **coherent detection**, which is discussed in Section 6.4.

The second special circumstance occurs when the user knows the timing of the signal. This means that the signal contains useful information only during a short window of time relative to a reference moment in time (trigger), whereas only noise is present outside this window. If prior knowledge about the timing is available, then it is feasible to design an instrument that measures the signal only during that window of time. The influence of noise would be significantly reduced.

Unfortunately, one often lacks access to a time reference that would enable synchronisation of a window of time in the detector. An exception is the measurement problem where the shape of the time-dependent signal of interest is known to be equal in shape to that of a reference signal, although with a time delay. The actual shape of the signals is not relevant, since the measurement information is contained in the time delay. Systems suitable for measuring on such signals are based on **correlation**. More detail is provided in Section 6.5.

Finally, the SNR can be improved by taking multiple measurements and applying (digital) signal processing. Although this is basically a filtering technique, it is discussed separately in Section 6.6.

6.2 Compensation and correction for error reduction

General instrumentation techniques to reduce the effect of internal and external noise sources are:

- Compensation
- Correction
- Feedback

6.2.1 Compensation

Compensation is used to reduce the effect of both additive and multiplicative errors. The principle of compensation is shown schematically in Fig. 6.1. In the case of additive errors (Fig. 6.1a), compensation involves the simultaneous measurement of both the intended quantity and the noise, using two measurement systems with unequal sensitivities to signal and noise. Simple calculus yields the intended value. A practical implementation is based on sensors that are equally susceptible to noise, but with unequal sensitivities to the intended signal. A simple subtraction yields the (attenuated) signal not affected by noise.

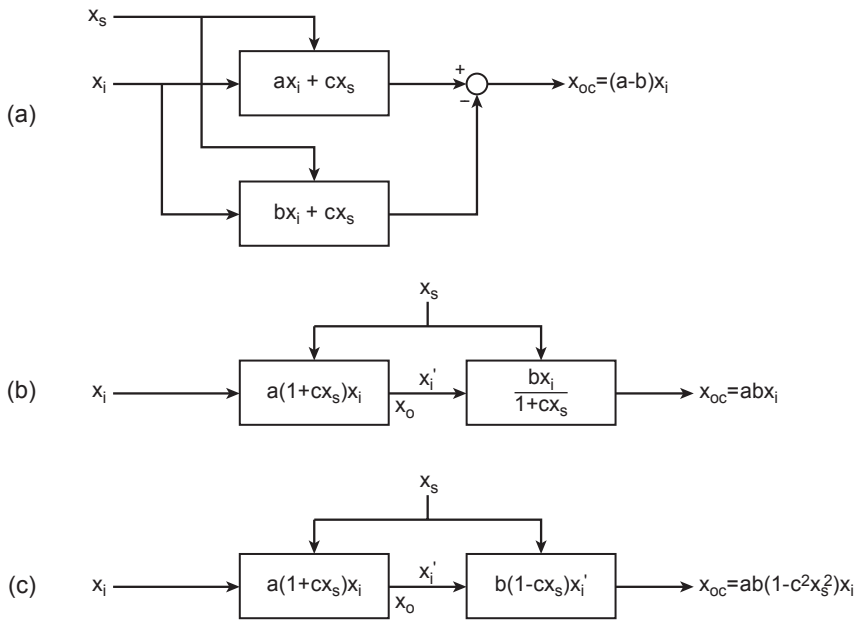

Figure 6.1, Compensation for: (a) additive errors, (b) multiplicative errors, (c) practical, although incomplete, compensation for multiplicative errors.

Example 6.1
A 6V silicon Zener diode exhibits a temperature coefficient (t.c.) of about +2mV/K. A conventional silicon diode operated at a forward bias has a voltage drop of about 0.6 V and t.c.= –2m V/K. A low-t.c. voltage reference can be realised by connecting these devices in series and applying a suitable bias current. This is a straightforward implementation of Fig. 6.1a.

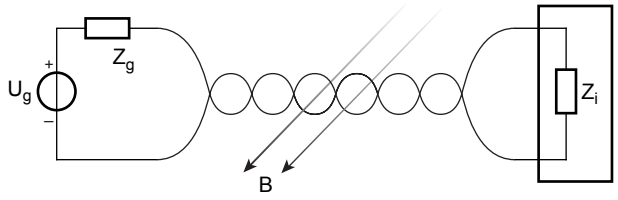

Figure 6.2, Compensation to reduce magnetic coupling by 'twisting' the two signal wires.

Example 6.2
Magnetic induction, as discussed in Section 5.6 (Fig. 5.25), is significantly reduced by twisting the two wires, as shown in Fig. 6.2. The overall induced voltage is equal to the sum of the loop voltages. As the induced

voltages in two adjacent loops are of opposite polarity, the induced voltages compensate at a equal loop cross-sectional area.

Multiplicative (scale) errors are compensated in the case of two blocks in cascade; one has a certain transfer function for the intended signal and the noise, while the other has the same sensitivity for the intended signal and the inverse sensitivity for the error signal, as is shown schematically in Fig. 6.1b.

The inverse transfer function is often difficult to realise. Therefore, an approach is presented in Fig. 6.1c that can be used to provide (partial) compensation for scale errors.

Compensation has a threefold meaning in the DC-operated Wheatstone bridge configuration shown in Fig. 6.3, which is applied for the read-out of strain gauges.

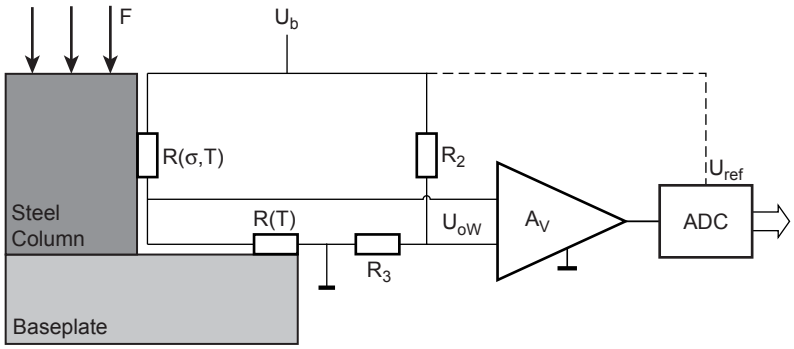

Figure 6.3, Temperature compensation for force measurement using strain gauges in a Wheatstone bridge.

In the balanced bridge (i.e. no strain in either strain gauge) the bridge output voltage is equal to: $U_o = U_b/2 - U_b/2 = 0$. In principle this bridge is composed of a measurement branch (with $R(\sigma,T)$ and $R(T)$) and a compensating branch (with $R_2 = R_3 = R$). The bridge itself, therefore, provides compensation for the additive common-mode term $U_b/2$ (this is the first interpretation).

The strain gauge is designed to measure strain. However is also a temperature-dependent resistor. One strain gauge is mounted on the structure thus making it sensitive to strain and temperature. The second strain gauge is mounted on the base and registers temperature changes only. The measurement branch, therefore, compensates for temperature (this is the second interpretation). The resistors in the compensating branch should for this reason also be kept at the same temperature.

Finally, the transfer from bridge imbalance to bridge output voltage, U_o, is linearly dependent on the excitation voltage, U_b. Any variation in U_b is basically a scale error. Compensation techniques to eliminate this effect use U_b as both the bridge excitation voltage and the reference voltage in the AD converter. The binary code is defined as a fraction of $U_{ref} = U_b$, which thus compensates for any variation (this is the third interpretation). This technique is referred to as a bridge with a **ratiometric** digital output.

6.2.2 Correction

Correction requires two separate measurements: in the first the intended quantity (signal) plus the error (noise) is measured, and in the second only the error (noise) is measured.

Correction has two advantages:

- It is easy to implement and does not require extensive knowledge on how the interfering signal is introduced
- It can be easily added to an existing setup.

However, correction requires two complete data-acquisition channels. Moreover, any uncertainty introduced in one of these channels does reduce the effectiveness of the correction.

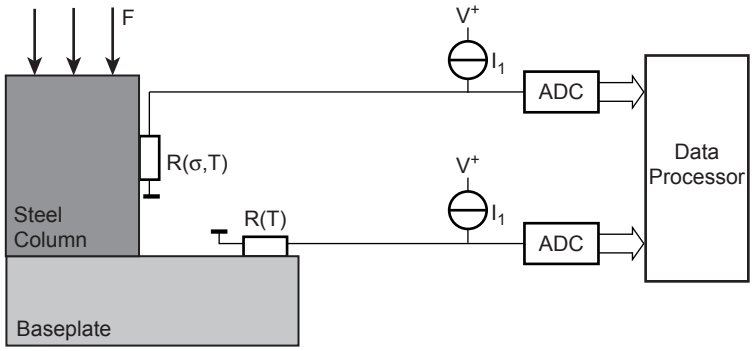

Figure 6.4, Correction for temperature effects.

Figure 6.4 shows the implementation of correction in a strain measurement. The voltages $I_1R(\sigma,T)$ and $I_1R(T)$ are measured and converted into a digital code. Subsequently, the processor calculates the strain, corrected for temperature. Since compensation is implemented at the front-end part of the data-acquisition channel, it usually suppresses the undesirable effect more effectively.

6.3 Feedback for error reduction

6.3.1 General principle of feedback

Feedback can be used to reduce the effect of both additive and scale errors. The basic principle is shown schematically in Fig. 6.5. A fraction β of the output signal, U_o, is subtracted from the input signal, U_i, which results in: $U_o = (U_i - \beta U_o)H$. Therefore, the transfer function is described by:

$$H_f = \frac{U_o}{U_i} = \frac{H}{1+H\beta}, \tag{6-1}$$

where βH is referred to as the closed-loop gain.

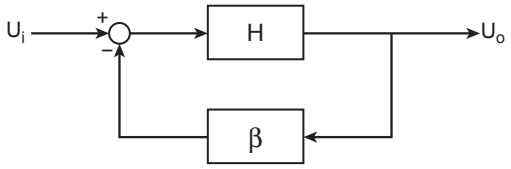

Figure 6.5, Feedback.

Note:
Notation in electronics often anticipates the use of an inverting amplifier to implement H. In this case the polarity of H is negative, thus $\beta H<0$ and the feedback signal is added to the input signal. The transfer function is described as: $H_f = H/(1-\beta H)$. This alternative description is easily recognised when checking the polarity of H and H_f.

For $\beta H \gg 1$, the transfer function is approximated by $H_f = 1/\beta$. This implies that the transfer is set by the feedback components only. This is the starting point of the OPAMP circuits described in previous Chapters. The accuracy of the transfer function of a feedback circuit is usually determined by the stability of the passive components. The relative error in an open-loop transfer function, H, with a nominal value H_o and tolerance ΔH ($H = H_o \pm \Delta H$), is equal to $\Delta H/H$. When implementing feedback, the resulting uncertainty in the transfer function (the relative error $\Delta H_f/H_f$) is described as:

$$\begin{aligned} &\frac{\Delta H_f}{\Delta H} \simeq \frac{\partial H_f}{\partial H} = \frac{\partial \dfrac{H}{1+\beta H}}{\partial H} = \frac{(1+\beta H)-\beta H}{(1+\beta H)^2} = \frac{1}{(1+\beta H)^2} = \frac{1}{1+\beta H} \times \frac{H_f}{H} \\ &\rightarrow \frac{\Delta H_f}{H_f} = \frac{\Delta H}{H} \times \frac{1}{1+\beta H} \simeq \frac{1}{H\beta} \times \frac{\Delta H}{H} \end{aligned} \tag{6-2}$$

The improved accuracy of the transfer function comes at the expense of a reduced system gain and stability. The transfer function decreases from H to $1/\beta$, and is thus reduced by the loop gain βH. This factor also determines the stability.

Example 6.3
An OPAMP has a nominal open-loop DC gain equal to: $A_o = 10^6$. However, the actual gain varies due to tolerances in the components used: $(\Delta A/A_o)_{max}$ = 50%. Feedback is used to set the gain to $H_f = 10^4$ (e.g. non-inverting amplifier). This transfer function is achieved at $\beta = 10^{-4}$, thus $\beta A_o = 100$. Therefore, a 50% change in A_o results in a 0.5% change in H_f.

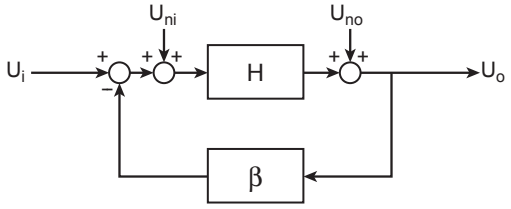

Figure 6.6, Use of feedback for reducing additive errors.

Feedback is also used to reduce the effect of additive sources of error. Figure 6.6 shows the structure of a generic feedback system, including error sources acting on the input, U_{ni}, (e.g. offset, input noise) and output, U_{no} (e.g. non-linear distortion due to saturation). The output signal is described by:

$$U_o = \frac{H}{1+H\beta}U_i + \frac{H}{1+H\beta}U_{ni} + \frac{1}{1+H\beta}U_{no} \tag{6-3}$$

This expression indicates that errors at the output of the open-loop gain stage are reduced by the loop gain. However, the error sources, U_{ni}, that are acting on the input are not distinguished from the input signals, U_i.

A major issue in the design of feedback systems is stability. The transfer function approaches infinity for $\beta H \sim -1$. Measures must be taken to ensure that a sufficient amplitude and phase margin are maintained, so that a -1 loop gain is not included at any frequency. A phase margin of 90^o is guaranteed in the case of a feedback composed of resistive components only. Additionally, an OPAMP is used with an open-loop gain described by a first-order system.

6.3.2 Feedback for reducing source loading

Feedback is a very suitable mechanism for modifying the input and output impedance of the overall system through design in order to reduce the error caused by source loading. The input impedance of a feedback amplifier is prima-

rily determined by the way the output is coupled to the inverting input (i.e. the subtraction node) and NOT by the physical input impedance of the OPAMP.

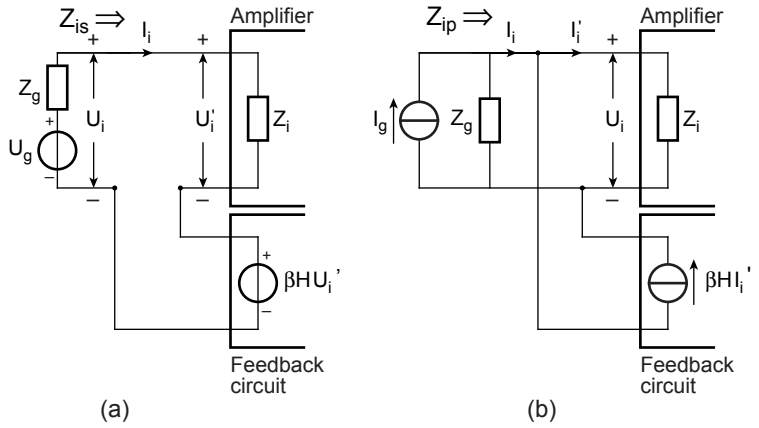

Figure 6.7, (a) Serial input coupling and (b) parallel coupling.

The first configuration is a circuit in which the input and output are voltage sources, as shown in Fig. 6.7a. The physical input impedance of the open-loop amplifier is Z_i. The feedback signal (i.e. the attenuated output signal) is connected in series with the input (note the polarity) to enable the voltage subtraction of U_i and $\beta U_o = \beta H U_i'$. Since the feedback signal is basically a replica of the input signal, it is intuitive to assume that the current flowing into the amplifier input is greatly reduced. Consequently, the input impedance, Z_{is}, is greatly increased as compared to Z_i, which is convenient in voltage read-out.

A more quantitative analysis of the series coupling shown in Fig. 6.7a results in:

$$
\begin{aligned}
&(1) \quad \rightarrow U_i' = U_i - H\beta U_i' \rightarrow U_i' = \frac{U_i}{1 + H\beta} \rightarrow U_i = (1 + H\beta)U_i' \\
&(2) \quad \rightarrow U_i' = I_i Z_i \rightarrow I_i = U_i'/Z_i \\
&\qquad Z_{is} = \frac{U_i}{I_i} = \frac{U_i'(1 + H\beta)}{U_i'/Z_i} = (1 + H\beta)Z_i
\end{aligned}
\tag{6-4}
$$

The input impedance of the feedback system with serial input coupling, Z_{is}, is equal to the physical input impedance of the amplifier, Z_i, multiplied by a factor equal to $1+H\beta$ (1 plus closed-loop gain).

The second configuration is a circuit in which the input and output are current sources, as shown in Fig. 6.7b. Subtraction is implemented using a parallel connection with the appropriate polarity. Since the feedback operation ensures that U_i is made as small as possible, the input impedance is greatly reduced, which is convenient in current source read-out Therefore, series coupling is used when the signal source is a voltage, and parallel coupling is implemented in the case of a current source read-out. Therefore, parallel coupling as shown in Fig. 2.59b results in:

$$\begin{aligned} &(1) \quad \rightarrow I_i' = I_i - H\beta I_i' = \frac{I_i}{1+H\beta} \rightarrow I_i = I_i'(1+H\beta) \\ &(2) \quad \rightarrow I_i' = \frac{U_i}{Z_i} \rightarrow U_i = I_i' Z_i \\ &Z_{ip} = \frac{U_i}{I_i} = \frac{I_i' Z_i}{I_i'(1+H\beta)} = \frac{Z_i}{1+H\beta} \end{aligned} \tag{6-5}$$

The input impedance of the feedback system with parallel input coupling, Z_{ip}, is equal to the physical input impedance, Z_i, divided by the factor 1+$H\beta$ (1 plus closed-loop gain).

These results are readily applicable to solve the problem of the reduced signal bandwidth in shielded cables, as described in Section 5.6. This effect is primarily due to the capacitance C_a between the inner cable and the shielding.

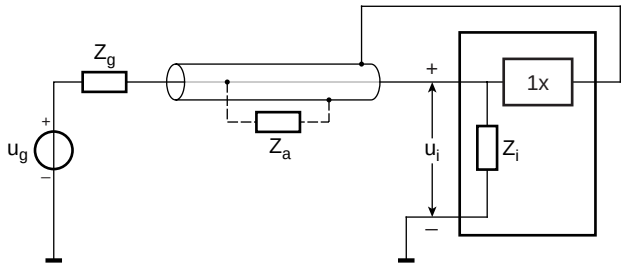

Figure 6.8, Active guarding to reduce capacitive coupling without reducing the input impedance.

The bandwidth reduction is avoided when using active guarding, as shown in Fig. 6.8. The 1× amplifier (also referred to as a **voltage follower** or **voltage buffer**) connects the shield (also referred to as the guard electrode) to the same potential as at the inner electrode. The output of the amplifier is a voltage source with a small source impedance and is almost as efficient as a ground contact in

the removal of the charge that is injected by EMI from the shield. The capacitance between the inner electrode and the shield has been made almost 'invisible'. Since the inner cable is surrounded by the active guarding electrode and the voltage difference is brought close to zero, no current flows. Consequently, the impedance between the inner electrode and shield is extremely high, which is equivalent to an extremely small capacitance.

It should be noted that this technique is in fact a direct implementation of the series coupling configuration shown in Fig. 6.7a. Basically, the shielding electrode is forced at $U_o=(1-\varepsilon)U_i$. The impedance between the inner signal cable and the shielding electrode is, by definition, equal to the ratio between their potential difference and the resulting current: $I_a'= (U_i-U_o)/Z_a= \varepsilon U_i/Z_a$.

The impedance between the inner conductor and the cable inner shield, Z_a', is defined as: $Z_a'= (U_i/i_a')$. Therefore, $Z_a'= Z_a/\varepsilon$, which is in agreement with Eqn. 6-4. The deviation from unity in the voltage follower transfer function, ε, should be as small as possible. However, the potential at the shield should under all circumstances be smaller than the potential at the inner cable to avoid positive feedback and instability. For this reason some margin is required.

6.3.3 Input impedance of OPAMP-based circuits

Equations 6-4 and 6-5 can be used to derive expressions for the input impedance of opamp-based feedback circuits. First, the non-inverting amplifier shown in Fig. 6.9 is considered, which is basically a feedback circuit with series coupling.

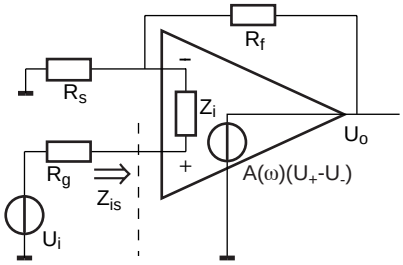

Figure 6.9, Input impedance of a non-inverting amplifier with an OPAMP open-loop gain described by: $A(\omega)= A_o/(1+j\omega\tau_v)$ and an open-loop input impedance $Z_i= R_i/(1+j\omega R_i C_i)$.

Calculating the input impedance involves connecting an input voltage, U_i, and the calculation of the resulting current into the non-inverting input node, while considering the fact that the feedback tries to reproduce this input voltage at the inverting input:

$$
\begin{aligned}
U_+ &= U_i \\
U_- &= \frac{R_s U_o}{R_s + R_f} = \frac{R_s A(\omega)\left[U_i - U_-\right]}{R_s + R_f} \rightarrow U_- = \frac{R_s A(\omega)}{\left[A(\omega)+1\right]R_s + R_f} U_i \\
Z_{is} &= \frac{U_i}{I_i} = \frac{U_i}{(U_+ - U_-)/Z_i} = Z_i \frac{\left[A(\omega)+1\right]R_s + R_f}{R_s + R_f}
\end{aligned}
\tag{6-6}
$$

which yields:

$$
Z_{is} = \frac{R_i\left(\frac{\left[A_o+1\right]R_s + R_f}{R_s + R_f}\right)\left(1 + j\omega\tau_v \frac{R_s + R_f}{\left[A_o+1\right]R_s + R_f}\right)}{(1 + j\omega R_i C_i)(1 + j\omega\tau_v)} \simeq \frac{R_i \frac{A_o}{G_{fo}}\left(1 + j\omega\tau_v \frac{G_{fo}}{A_o}\right)}{(1 + j\omega R_i C_i)(1 + j\omega\tau_v)},
\tag{6-7}
$$

where $G_{fo} = (R_s+R_f)/R_s$ denotes the transfer function in the case of an ideal OPAMP ($A(\omega) = A_o \rightarrow \infty$).

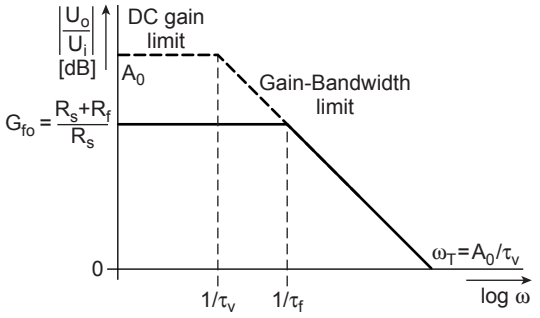

Figure 6.10, Modulus plot of the non-inverting amplifier.

As is shown in Fig. 6.10, the OPAMP can only be used to realise a frequency-dependent transfer function that fits within the open-loop gain: $G_f(\omega) \ll A(\omega)$ (see also Section 4.4.1). Since $A(\omega) = A_o/(1+j\omega\tau_v)$, two different operating regimes can be identified:

- the DC gain limited regime ($\omega < 1/\tau_v$) and
- the gain-bandwidth limited regime ($\omega > 1/\tau_v$).

As a result:

$$\begin{aligned}\omega < \frac{1}{\tau_v} : \frac{A_o}{G_{\text{fo}}} \gg 1 \rightarrow G_{\text{fo}} \ll A_o \\ \omega > \frac{1}{\tau_v} : \omega G_{\text{fo}} < \frac{A_o}{\tau_v} \rightarrow \omega_{\text{-3dB}} < \frac{A_o}{\tau_v G_{\text{fo}}}\end{aligned} \tag{6-8}$$

where $\omega_{\text{-3dB}} = 1/\tau_{\text{f}}$ denotes the -3 dB cut-off frequency of the non-inverting amplifier. Applying these restrictions to Eqn. 6-7 yields:

$$Z_{\text{is}} = \frac{R_i \dfrac{A_o}{G_{\text{fo}}\left(1 + j\omega\tau_v\right)}\left(1 + j\omega\tau_v \dfrac{G_{\text{fo}}}{A_o}\right)}{1 + j\omega R_i C_i} \simeq \frac{R_i \dfrac{A(\omega)}{G_{\text{fo}}}}{1 + j\omega R_i C_i} \tag{6-9}$$

For $\omega R_{\text{i}} C_{\text{i}} < 1$, the input impedance of the non-inverting amplifier is equal to the open-loop input resistance of the opamp, R_{i}, multiplied by the closed-loop gain, $A(\omega)ß = A(\omega)/G_{\text{fo}}$. For $\omega < 1/\tau_{\text{v}}$ the open-loop gain $A(\omega) = A_{\text{o}}$.

The input impedance, Z_{is}, of the feedback circuit is composed of a resistance, R_{is}, which is equal to the open-loop input resistance, R_{i}, connected in parallel to a capacitor, C_{is}. The expressions for the component result from Eqn. 6-9 in:

$$\begin{aligned}R_{\text{is}} &= R_i \frac{A(\omega)}{G_{\text{fo}}} = R_i \frac{A_o R_s}{R_{\text{s}} + R_{\text{f}}} \\ C_{\text{is}} &= C_i \frac{G_{\text{fo}}}{A(\omega)} = C_i \frac{R_{\text{s}} + R_{\text{f}}}{A_o R_s}\end{aligned} \tag{6-10}$$

For a typical OPAMP circuit, $1/\tau_{\text{v}} \ll (R_{\text{i}} C_{\text{i}})^{-1}$. Therefore, for $1/\tau_{\text{v}} < \omega < (R_{\text{i}} C_{\text{i}})^{-1}$ the open-loop gain $A(\omega) = A_{\text{o}}/j\omega\tau_{\text{v}}$. Consequently, $|Z_{\text{is}}|$ reduces with frequency in a way that is similar to the transfer function of a first-order low-pass filter.

Example 6.4
Increasing the input impedance by applying series feedback has the most profound effect in the case of unity-feedback ($G_{\text{v}}=1$). This is implemented in the non-inverting amplifier in Fig. 6.9 by short-circuiting R_{f} and omitting R_{s}. The voltage buffer is very suitable for sensor read-out in the case of a high, poorly reproducible, source impedance. Assume the following OPAMP specifications: $R_{\text{i}} = 2$ MΩ, $C_{\text{i}} = 0.5$ pF, $A_{\text{o}} = 100$ dB and a unity-gain frequency $f_{\text{T}} = 4$ MHz.

Calculate the input impedance, Z_{is}, of the voltage buffer as a function of frequency.

Solution:
$A_o = 10^5$ and $G_v = 1$.
$\tau_v = A_o/(2\pi \times f_T) = 10^5/(2\pi \times 4 \times 10^6) = 4$ ms.
$R_iC_i = (2 \times 10^6 \times 5 \times 10^{-13}) = 1$ μs.

For $f < 4$ MHz$/10^5 = 40$ Hz, $R_{is} = R_i \times A_o = 200$ GΩ and $C_{is} = C_i/A_o = 5$ aF. Note that $(2\pi \times 40 \times 5 \times 10^{-18})^{-1} = 800$ TΩ» R_{is}. Hence, the input impedance is resistive ($Z_{is} = R_{is} = 200$ GΩ) in this part of the spectrum.

At $f = (2\pi \times R_iC_i)^{-1} = 159$ kHz, $|Z_{is}| = R_iA_o/(2\pi f\tau_v\sqrt{2}) = 35.4$ MΩ.
For f» $(2\pi \times R_iC_i)^{-1}$ the input impedance $|Z_{is}| = R_iA_o/(4\pi^2 f^2 \tau_v R_iC_i)$ and decreases by a factor 100 per decade increase in frequency.

At the unity-gain frequency, $\omega_T = A_o/\tau_v$, the input impedance is described by: $|Z_{is}| = (\omega_T C_i)^{-1}$. This implies that the input impedance is fully determined by the open-loop input capacitance and is unaffected by the feedback. This result is in agreement with the fact that the loop gain has reduced to a factor 1. As is indicated in Fig. 6.10, a feedback circuit should be designed within the open-loop gain of the OPAMP used. The area under the magnitude plot of the open loop gain is the available spectral design space.

The input impedance, Z_{ip}, in the case of parallel coupling is an important performance parameter for the current-to-voltage converter (trans-impedance circuit). The expression for Z_{ip} is found with a similar approach used for series coupling in the non-inverting amplifier. The potential at the inverting input, U_-, in Fig. 6.11 due to the input current, I_s, is calculated, thus Z_{ip} results in:

$$\left.\begin{aligned} Z_{ip} &= \frac{U_-}{I_s} = \frac{U_-}{I_f + I_i} \\ I_f &= \frac{U_- - U_o}{Z_f} = \frac{U_- - A(\omega)[U_+ - U_-]}{Z_f} = [A(\omega)+1]\frac{U_-}{Z_f} \\ I_i &= \frac{U_+ - U_-}{Z_i} = \frac{U_i}{Z_i} \end{aligned}\right\} \rightarrow$$
$$Z_{ip} = \frac{1}{\frac{1}{Z_i} + \frac{1 + A(\omega)}{Z_f}} = \frac{Z_iZ_f}{[A(\omega)+1]Z_i + Z_f} \approx \frac{Z_f}{A(\omega)} \qquad (6\text{-}11)$$

Recognising that for the trans-impedance amplifier used $Z_i = R_i/(1+j\omega R_iC_i)$, $Z_f = R_f$ and $A(\omega) = A_o/(1+j\omega\tau_v)$ yields: $Z_{ip} = R_{ip} + j\omega L_{ip} = (R_f/A_o) + j\omega(\tau_v R_f/A_o)$.

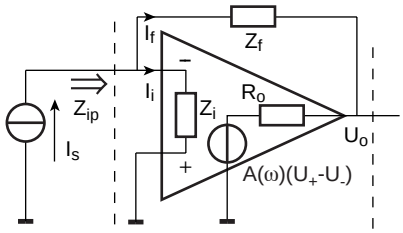

Figure 6.11, Input impedance of the trans-impedance circuit, with $Z_i = R_i/(1+j\omega R_i C_i)$, $Z_f = R_f$ and $A(\omega) = A_o/(1+j\omega\tau_v)$.

The input impedance is inductive over a large part of the spectral operating range. This property may result in complications for a source with a significant source capacitance, as is the case in reverse-biased photodiode read-out. A careful design, therefore, requires an analysis of a possible resonance due to $L_{ip}C_p$, which would strongly affect the accuracy of the read-out transfer function.

The input impedance of the trans-impedance circuit is also very important in a charge amplifier, which is characterised by a minimum operating frequency $\omega_{min} = \max\{1/\tau_v, (R_f C_f)^{-1}\}$, a maximum operating frequency $\omega_{max} = A_o/\tau_v$ and $Z_i = R_i/(1+j\omega R_i C_i)$, $Z_f = (j\omega C_f)^{-1}$. Consequently, the open-loop gain approximated by: $A(\omega) = A_o/j\omega\tau_v$. Applying Eqn. 6-11 yields:

$$Z_{ip} \approx \frac{Z_f}{A(\omega)} = \frac{\frac{1}{j\omega C_f}}{\frac{A_o}{j\omega\tau_v}} = \frac{\tau_v}{A_o C_f} \tag{6-12}$$

This resistive input impedance limits the performance of the current summation node at U_-, which is essential in the read-out of differential capacitive transducers, as shown in Fig. 6.12 for the vertical displacement sensor.

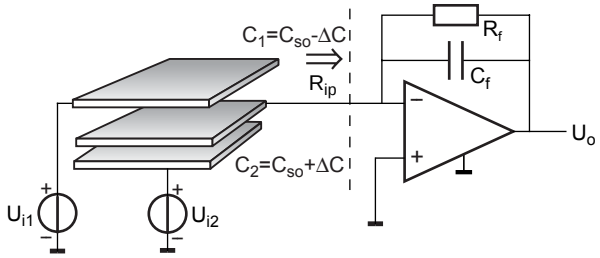

Figure 6.12, Read-out of the capacitive accelerometer using a charge amplifier.

In Section 5.6 (Fig. 5.22) the inverting input is considered a suitable node for perfect current addition, which implies a (virtual) voltage source at ground

potential with zero source impedance at this node. However, a non-zero input impedance of the charge amplifier introduces a scale error and frequency dependence. Assuming the other specifications of the OPAMP to be ideal and u_{i1}= -u_{i2}= u_i, results in a current flowing towards the OPAMP described by:

$$i_{R_{ip}} = \frac{u_{i1} \times j\omega C_1}{1 + j\omega R_{ip}\left(C_1 + C_2\right)} + \frac{u_{i2} \times j\omega C_2}{1 + j\omega R_{ip}\left(C_1 + C_2\right)} = -u_i \frac{2\, j\omega \Delta C}{1 + j\omega 2 R_{ip} C_{so}} \qquad (6\text{-}13)$$

This results in the transfer function:

$$u_o = -i_{R_{ip}} \times \frac{1}{j\omega C_f} = 2u_i \frac{\Delta C / C_f}{1 + j\omega 2 R_{ip} C_{so}} = 2u_i \frac{\Delta C / C_f}{1 + j\omega 2\tau_v C_{so} / A_o C_f} \qquad (6\text{-}14)$$

This expression introduces another limitation in operating frequency in addition to the open-loop bandwidth of the OPAMP. The denominator term in eqn. 6.14 implies that the operating frequency is limited to; $\omega = (2R_{ip}C_{so})^{-1} = A_o C_f / (2\tau_v C_{so}) = \omega_T (C_f / 2C_{so})$. Since $\Delta C / C_{so} \ll 1$, Eqn. 6.14 implies that $C_f < C_{so}$ should be satisfied for an acceptable sensitivity for $\Delta C / C_f$. However, a small C_f / C_{so} is difficult to achieve using practical components for C_f when also considering the fact that a typical sensor capacitance is in the order of magnitude of C_{so}= 1 pF. Moreover, minimising C_f / C_{so} would also limit the excitation frequency to: $\omega_{max} = \omega_T (C_f / 2C_{so}) \ll \omega_T$.

6.3.4 Output impedance of OPAMP-based circuits

Feedback can also be used to control the output impedance through design. A voltage amplifier with a low output impedance reduces any susceptibly to loading by a subsequent stage.

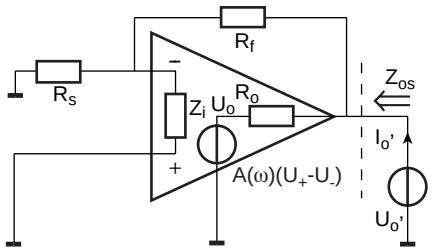

Figure 6.13, Output impedance of the non-inverting amplifier with an opamp open-loop described by: $A(\omega) = A_o / (1 + j\omega\tau_v)$.

The calculation of the output impedance, Z_{os}, of the feedback circuit is based on the following theoretical consideration: Assume a voltage source U_o' is connected directly to the output, as shown in Fig. 6.13. As a result, current I_o' would flow, which is composed of two components: one flowing into the open-loop OPAMP output resistance R_o and the other into the feedback resistance R_f. From

these considerations the output impedance of the feedback circuit can be derived as:

$$\left.\begin{aligned} I_o' &= \frac{U_o'-U_o}{R_o}+\frac{U_o'-U_-}{R_\mathrm{f}} = U_o'\left(\frac{1}{R_o}+\frac{1}{R_\mathrm{f}}+\frac{U_o}{U_o'}\frac{1}{R_o}+\frac{U_-}{U_o'}\frac{1}{R_\mathrm{f}}\right)\\ \left.\begin{aligned} U_- &= \frac{R_s}{R_s+R_\mathrm{f}}U_o'\\ U_o &= -A(\omega)U_- \end{aligned}\right\} &\rightarrow \frac{U_o}{U_o'} = -A(\omega)\frac{R_s}{R_s+R_\mathrm{f}} \end{aligned}\right\}\rightarrow$$

$$I_o' = U_o'\left(\frac{1}{R_o}+\frac{1}{R_\mathrm{f}}+\frac{A(\omega)R_s}{R_o(R_s+R_\mathrm{f})}-\frac{R_s}{R_\mathrm{f}(R_s+R_\mathrm{f})}\right) \qquad (6\text{-}15)$$

$$Z_{os} = \frac{U_o'}{I_o'} = \frac{R_o}{1+\frac{R_o}{R_\mathrm{f}}+\frac{A(\omega)R_s}{R_s+R_\mathrm{f}}-\frac{R_oR_s}{R_\mathrm{f}(R_s+R_\mathrm{f})}} \approx R_o\frac{G_{\mathrm{f}o}}{A(\omega)}$$

Hence, the output impedance of the feedback circuit is equal to the open-loop output resistance divided by the loop gain. The output impedance is reduced, which is in general a favourable property when the output should be a voltage source. The output impedance is the source impedance from the perspective of a subsequent gain stage. Therefore, any scale error due to loading is reduced with the output impedance of the first stage. It should be noted that for $\omega > 1/\tau_\mathrm{v}$ the output impedance is inductive ($L_\mathrm{os} = \tau_\mathrm{v} R_\mathrm{o} G_\mathrm{fo}/A_\mathrm{o}$). Care should be taken to avoid resonance in the case of a highly capacitive output load.

Since R_s and R_f are not significant in the expression for Z_os, it can be concluded that, unlike the input impedance (see Fig. 6.7), the output impedance does not depend on whether serial or parallel input coupling is used in the feedback.

Both the non-inverting amplifier and the current-to-voltage inverter have the same output impedance.

The scale error introduced due to the combined effect of both source loading by the input of a read-out circuit and loading of the output of this circuit by a load, as shown in Fig. 6.14, can be calculated using the expressions derived in this section. The source loading error results from the specified source impedance, Z_g, and the input impedance of that circuit at the specified operating frequency range, Z_is (or Z_ip in the case of current source read-out). The scale error due to loading of the circuit with output impedance Z_os and a load imposed by the subsequent stage is specified as Z_L, can be calculated.

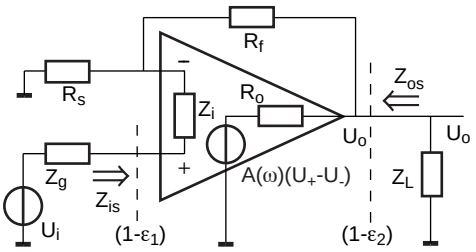

Figure 6.14, Analysing the effect of source and output loading in a non-inverting amplifier using an opamp with $Z_i = R_i/(1+j\omega R_i C_i)$ and $A(\omega) = A_o/(1+j\omega\tau_v)$.

6.4 Coherent detection

6.4.1 From frequency filtering to coherent detection

Frequency filtering is widely used in measurement systems to improve the SNR and is described in Section 2.4.3. In the case of a relatively narrowband input signal contained in wideband noise (e.g. Wheatstone bridge output with white noise), filtering is applied to improve the signal-to-noise ratio by selective attenuation of the out-of-band noise components (e.g. a high-pass filter (HPF) for stray light reduction as in Example 6.5).

Alternatively, in the case of a wideband input signal with a spectrally well-defined, narrowband noise component of high amplitude (e.g. capacitively coupled mains voltage at 50 Hz), the purpose of filtering is to selectively attenuate the in-band noise component with a minimum loss of signal content.

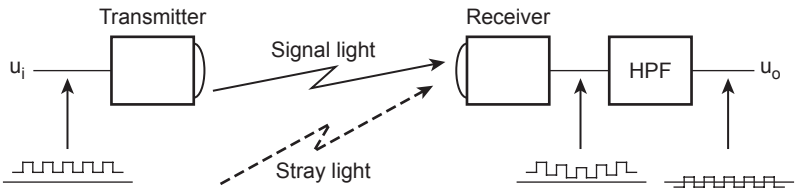

Figure 6.15, Source modulation and frequency-selective detection in an optical displacement measuring system with reduced sensitivity to environmental stray light.

Example 6.5

An optical distance measurement system is based on a Light Emitting Diode (LED), which irradiates pulsed light of a well-known frequency, and a photodiode detector (Fig. 6.15). The photo current decreases with the square of the distance between the LED and the diode. The dominant source of error is low-frequency stray light. The pulsed signal (> 1 kHz)

enables the light originating form the LED to be distinguished from stray light (e.g. 100 Hz from a light bulb), using a simple HPF.

Filtering becomes challenging when the signal is characterised by a very narrow bandwidth around a central frequency. A high-Q bandpass filter (BPF) is required, which is difficult to realise reproducibly. Moreover, the central frequency of the signal may drift over time. The resulting shift in the central frequency could be larger than the filter bandwidth. As a consequence the bandwidth of the bandpass filter has to remain relatively wide to ensure coverage of the entire bandwidth of the desirable signal under all practical circumstances. However, the wider band also results in a relatively high in-band noise power.

This problem could be resolved if one were able to track this central frequency and subsequently to feed the signal through a very narrow band filter with a resonance frequency that is adapted to this actual central frequency. Tracking of the centre frequency is possible when it is also being used as the excitation frequency, such as in the AC-operated Wheatstone bridge. The AC-excitation can be considered a modulation technique that shifts the measurement signal spectrum away from the low-frequency part of the spectrum that contains strong noise sources (e.g. 50 Hz EMI, 1/f noise) to higher frequencies. De-modulation is used after signal processing to retrieve the original signal. This technique enables the detection of highly corrupted signals based on knowledge about the modulation frequency. The practical implementation of this technique is referred to as **coherent detection**.

Coherent detection is a powerful instrumentation technique for amplitude measurement of a signal with a very poor SNR when the measurement setup makes use of AC excitation. The AC-operated Wheatstone bridge, the AC-operated differential capacitive transducer with a charge amplifier for the read-out and the optical detector with chopping of the light source are all examples of such a system. The AC-excitation makes it possible to eliminate the effect of offset in the Wheatstone bridge read-out and that of environmental light in the optical detector. In both measurement systems the frequency of the excitation source is physically available for use in the read-out circuit.

Figure 6.16 shows how coherent detection is implemented to read-out the AC-operated Wheatstone bridge. The imbalance in a full bridge results in a differential voltage, which is amplified in a differential amplifier with offset and a finite *CMRR*. The amplifier output signal is subsequently multiplied with the excitation voltage, and the DC-component is selected using an LPF.

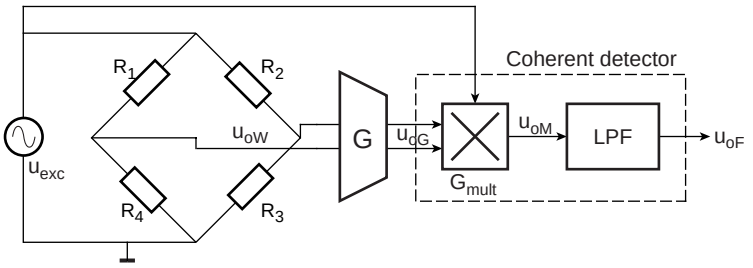

Figure 6.16, Read-out of a Wheatstone bridge using coherent detection.

The amplified bridge output signal, $u_{oG}= G\hat{u}_{exc}(\Delta R/R)\sin(\omega_{exc}t+\varphi)$ is multiplied with the excitation signal, $u_{exc}= \hat{u}_{exc}\sin(\omega_{exc}t)$, and the low-frequency component of the product is determined using an LPF. Operation is based on the orthogonality of two (co)-sine functions. Using basic goniometrical relations yields a voltage at the output of the multiplier that is expressed as:

$$u_{oM} = G_{mult} \times G \times \left\{ \left(\frac{\Delta R}{R} \right) \hat{u}_{exc} \sin\left(\omega_{exc} t + \varphi\right) \right\} \times \hat{u}_{exc} \sin\left(\omega_{exc} t\right) = \\ G_{mult} G \frac{\hat{u}_{exc}^2}{2} \frac{\Delta R}{R} \left[\cos\left(\left(\omega_{exc} - \omega_{exc}\right) t + \varphi \right) - \cos\left(\left(\omega_{exc} + \omega_{exc}\right) t - \varphi \right) \right], \tag{6-16}$$

where G_{mult} denotes the conversion gain of the multiplier $[\mathrm{V}]^{-1}$, G the gain of the differential amplifier and φ the phase shift due to the differential amplifier. Low-pass filtering at $\omega_{LPF} \ll \omega_{exc}$ results in a DC voltage U_{oF}:

$$U_{oF} = G G_{mult} G_{LPF} \frac{\hat{u}_{exc}^2}{2} \frac{\Delta R}{R} \cos\left(\varphi\right), \tag{6-17}$$

where G_{LPF} is the DC gain of the LPF. This expression assumes a static bridge output signal. In a practical instrument, ΔR could be due to a strain gauge being dynamically loaded by a mechanical force. The strain gauge, therefore, has a certain (mechanical) bandwidth, $S(f)$, as is shown in Fig. 6.17.

Clearly, DC-excitation gives an unfavourable SNR, which can be greatly improved when using AC-excitation and coherent detection to retrieve the low-frequency spectrum after signal amplification. In the case of a mechanical strain component ε at frequency ω_ε, $\varepsilon(\omega_\varepsilon)$, and a gauge factor of k_ε, the bridge imbalance $(\Delta R/R)u_{exc}(\omega_{exc})= k_\varepsilon\varepsilon(\omega_\varepsilon)u_{exc}(\omega_{exc})$ also contains this spectral component. The output signal of the differential amplifier for $\omega_\varepsilon \ll \omega_{exc}$ (assuming a frequency independent phase shift) is expressed as:

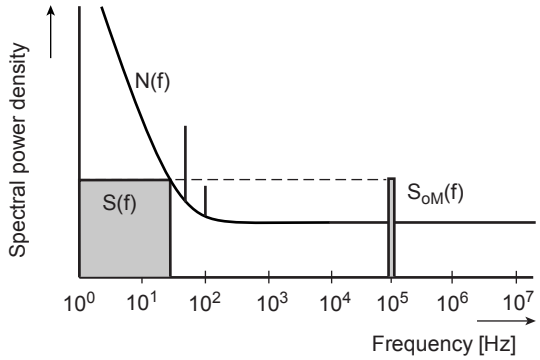

Figure 6.17, Spectrum of the input signal, $S(f)$, for DC excitation and noise, $N(f)$, and the same input signal for multiplication with an excitation signal at 100 kHz, $S_{OM}(f)$.

$$u_{oG} = G \times \hat{u}_{exc} \left\{ k_\varepsilon \hat{\varepsilon} \cos(\omega_\varepsilon t) \right\} \sin(\omega_{exc} t + \varphi) = \\ G \frac{\hat{u}_{exc} k_\varepsilon \hat{\varepsilon}}{2} \left[\sin\left((\omega_{exc} + \omega_\varepsilon) t + \varphi \right) + \sin\left((\omega_{exc} - \omega_\varepsilon) t + \varphi \right) \right], \tag{6-18}$$

which is basically the spectrum of an amplitude-modulated signal with a suppressed carrier, ω_{exc}. Applying this AM-modulated signal to the input of the coherent detector, and using the same approach as taken in the derivation of Eqn. 6-16, yields an expression for the output voltage after multiplication:

$$u_{oM} = G_{mult} \times \\ G \frac{\hat{u}_{exc} k_\varepsilon \hat{\varepsilon}}{2} \left[\sin\left((\omega_{exc} + \omega_\varepsilon) t + \varphi \right) + \sin\left((\omega_{exc} - \omega_\varepsilon) t + \varphi \right) \right] \times \hat{u}_{exc} \sin(\omega_{exc} t) = \\ G_{mult} G \frac{\hat{u}_{exc}^2 k_\varepsilon \hat{\varepsilon}}{4} \left[2\cos(\omega_\varepsilon t)\cos(\varphi) - \cos\left((2\omega_{exc} + \omega_\varepsilon) t + \varphi \right) - \cos\left((2\omega_{exc} - \omega_\varepsilon) t + \varphi \right) \right] \tag{6-19}$$

Low-pass filtering at $\omega_\varepsilon \ll \omega_{LPF} \ll \omega_{exc}$ results in:

$$U_{oF} = G G_{mult} G_{LPF} \frac{\hat{u}_{exc}^2 k_\varepsilon \hat{\varepsilon}}{2} \cos(\omega_\varepsilon t) \cos(\varphi) \tag{6-20}$$

Therefore, an electrical signal proportional to the strain is available at the output of the low-pass filter. This data acquisition system provides a gain of $G_{tot} = G G_{mult} G_{LPF} \hat{u}_{exc}^2 k_\varepsilon / 2$. This may appear to be a roundabout way of implementing gain. However, it offers a significant advantage, which is the strongly reduced sensitivity to offset in the differential amplifier.

The spectral band of interest in a mechanical measurement system usually includes very low-frequency components. The DC transfer function is very important, hence offset is a limiting factor for direct read-out of the strain gauge using DC excitation. The equivalent input offset voltage of the differential amplifier results after multiplication in a spectral component at the excitation frequency:

$$u_{oM} = G_{mult} \times G \times \left\{ \left(\frac{\Delta R}{R} \right) \hat{u}_{exc} \sin\left(\omega_{exc} t + \varphi\right) + U_{os} \right\} \times \hat{u}_{exc} \sin\left(\omega_{exc} t\right) =$$

$$G_{mult} G \left[\frac{\hat{u}_{exc}^2}{2} \frac{\Delta R}{R} \cos\left(\varphi\right) + U_{os} \hat{u}_{exc} \sin\left(\omega_{exc} t\right) \right] \rightarrow \tag{6-21}$$

$$U_{oF} = G_{mult} G \frac{\hat{u}_{exc}^2}{2} \frac{\Delta R}{R} \cos\left(\varphi\right)$$

Offset in the differential amplifier acts as a DC-scale factor of the excitation voltage after multiplication, which is removed in the LPF and no longer imposes a detection limitation.

The same mechanism substantially reduces the susceptibility of the measurement to 1/f noise. It should be noted that an offset voltage at both inputs of the multiplier results in a DC output voltage, which is one of the factors that sets the detection limit in a coherent detector, as is discussed in the next section.

The noise bandwidth in the coherent detector is defined by the cut-off frequency of the LPF.

Although a BPF can also be used to achieve the narrowband operation required for low noise, such an approach requires a bandpass filter with unrealistically high values for the quality factor, Q. In the case of a mechanical spectrum that is limited to ω_ε, and an excitation frequency $\omega_{exc} \gg \omega_\varepsilon$, the BPF should be designed for a resonance frequency at ω_{exc} and a quality factor $Q = \omega_{exc}/2\omega_\varepsilon \gg 1$.

6.4.2 Detection limit in a practical coherent detector

The coherent detector introduced in the previous section features ideal properties. The performance of a practical coherent detector is limited by the multiplier, which has:

- non-linearities in the reference channel,
- non-linearities in the input channel and
- non-linearities in the output stage.

Also the equivalent input-referred offset voltage sources have to be considered. It should be noted that, unlike in a linear component, such as an amplifier, the offset in a multiplier cannot be adequately represented by equivalent offset sources in one channel only. The zero offset in the other channel after multiplication would simply result in a zero offset at the output irrespective of the values of these equivalent sources of offset. Hence, offset is usually specified at the output.

The detection limit in a coherent detector is due to the combined effect of these three sources of error. These limitations will be discussed one by one.

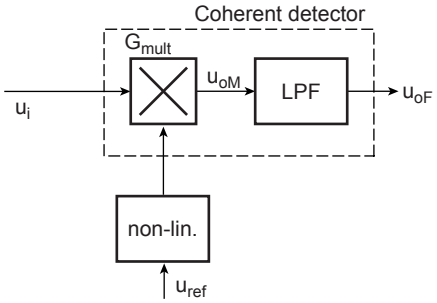

Figure 6.18, Coherent detector with non-linearity in the reference channel.

First the reference channel is assumed to generate non-linear distortion, whereas all other properties of the multiplier are considered ideal. In Fig. 6.18 the non-linearity of the reference channel is represented by a separate block at the input of the multiplier. The resulting transfer function of the multiplier is expressed as:

$$\begin{aligned} u_{oM} &= G_{mult}\left[u_r \times u_i\right] = \\ &G_{mult}\left[\left(\hat{u}_r \cos\left(\omega_r t\right) + \beta_2 \hat{u}_r \cos^2\left(\omega_r t\right) + \beta_3 \hat{u}_r \cos^3\left(\omega_r t\right) + ...\right) \times \hat{u}_i \cos\left(\omega_i t\right)\right], \end{aligned} \tag{6-22}$$

where β_i denotes the i^{th}-order distortion in the reference channel. Assuming, for the sake of simplicity, second-order distortion only yields:

$$\begin{aligned} u_{oM} &= G_{mult}\left[\left(\hat{u}_r \cos\left(\omega_r t\right) + \beta_2 \hat{u}_r \cos^2\left(\omega_r t\right)\right) \times \hat{u}_i \cos\left(\omega_i t\right)\right] = \\ &G_{mult}\left[\left(\hat{u}_r \cos\left(\omega_r t\right) + \frac{\beta_2 \hat{u}_r}{2}\left(1 + \cos\left(2\omega_r t\right)\right)\right) \times \hat{u}_i \cos\left(\omega_i t\right)\right] = \\ &G_{mult}\frac{\hat{u}_r \hat{u}_i}{2}\left[\cos\left(\left(\omega_r \pm \omega_i\right)t\right) + \beta_2 \cos\left(\omega_i t\right) + \frac{\beta_2}{2}\cos\left(\left(2\omega_r \pm \omega_i\right)t\right)\right] \end{aligned} \tag{6-23}$$

LP filtering with $\omega_{LPF} \ll \omega_r$ results in a coherent detector response equal to:

$$u_{oF} = G_{LPF} G_{mult} \frac{\hat{u}_r \hat{u}_i}{2} \left[\cos\left((\omega_r - \omega_i) t \right) + \frac{\beta_2}{2} \cos\left((2\omega_r - \omega_i) t \right) \right] \tag{6-24}$$

The first term indicates the desired response, whereas the second term indicates a parasitic sensitivity to a frequency component in the input signal at frequency $\omega_i = 2\omega_r$. The second-order non-linearity in the reference channel, therefore, generates a sensitivity of the coherent detector to a spectral component in the input channel at the double frequency. The same applies to the third harmonic distortion, which results in a sensitivity of the coherent detector to $\omega_i = 3\omega_r$.

In general, non-linear distortion in the reference channel results in sensitivity to *super-harmonics* in the input channel.

This can also be explained with a simple qualitative inspection of the coherent detector operation. Since the coherent detector is sensitive to any spectral component that causes a DC component at the output, any spectral component shared by the input signal and reference signal is detected. Hence, the presence of the double frequency in the reference channel makes the coherent detector sensitive to $\omega_i = 2\omega_r$ in the input channel. Since this part of the spectrum of the input signal contains noise only, the SNR is reduced.

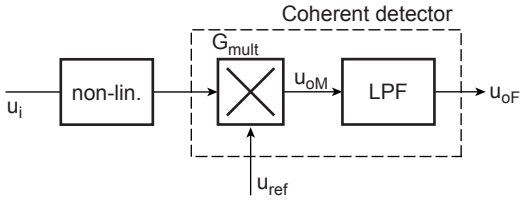

Figure 6.19, Coherent detector with non-linearity in the input channel.

The second limitation of the multiplier is non-linearity in the input channel, as shown in Fig. 6.19. The effect on the coherent detector response can be analysed in a similar way as used for the analysis of the reference channel:

$$\begin{aligned} u_{oM} &= G_{mult} \left[u_r \times u_i \right] = \\ &G_{mult} \left[\hat{u}_r \cos(\omega_r t) \times \hat{u}_i \left(\cos(\omega_i t) + \gamma_2 \cos^2(\omega_i t) + \gamma_3 \cos^3(\omega_i t) + \ldots \right) \right], \end{aligned} \tag{6-25}$$

where γ_i denotes the i^{th}-order distortion in the input channel. In the case of only a second-order distortion, this expression simplifies to:

$$\begin{aligned} u_{oM} &= G_{mult}\left[\hat{u}_r\cos(\omega_r t)\times\left(\hat{u}_i\cos(\omega_i t)+\gamma_2\hat{u}_i\cos^2(\omega_i t)\right)\right]= \\ &G_{mult}\left[\hat{u}_r\cos(\omega_r t)\times\left(\hat{u}_i\cos(\omega_i t)+\frac{\gamma_2\hat{u}_i}{2}\left(1+\cos(2\omega_i t)\right)\right)\right]= \\ &G_{mult}\frac{\hat{u}_r\hat{u}_i}{2}\left[\cos\left((\omega_r\pm\omega_i)t\right)+\gamma_2\cos(\omega_r t)+\frac{\gamma_2}{2}\cos\left((\omega_r\pm 2\omega_i)t\right)\right] \end{aligned} \tag{6-26}$$

Low-pass filtering with $\omega_{LPF} \ll \omega_r$ results in a coherent detector response:

$$u_{oF} = G_{LPF}G_{mult}\frac{\hat{u}_r\hat{u}_i}{2}\left[\cos\left((\omega_r-\omega_i)t\right)+\frac{\gamma_2}{2}\cos\left((\omega_r-2\omega_i)t\right)\right] \tag{6-27}$$

The first term indicates the desired response, whereas the second term indicates a parasitic sensitivity to a frequency component in the input signal at $\omega_i = \omega_r/2$. The second-order non-linearity in the input channel generates a spectral component at the double frequency. Therefore, a spectral component in the input voltage at half the frequency of the reference voltage is detected. Similarly, a third harmonic distortion results in a sensitivity of the coherent detector to $\omega_i = \omega_r/3$.

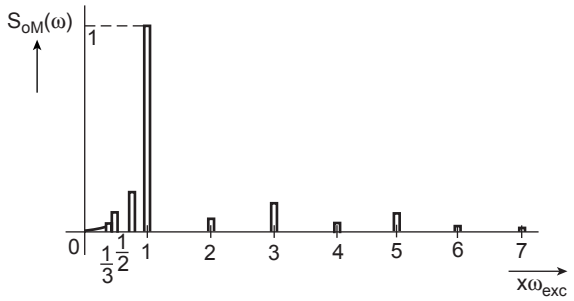

Figure 6.20, Spectral sensitivity of a practical coherent detector due to non-linearities in the input- and reference channel.

In general, a non-linearity in the input channel results in a sensitivity to *sub-harmonics* in the input channel.

The combined effect of harmonic distortion in the input channel and reference channel results in a spectral sensitivity for the input signal, as is shown in Fig. 6.20.

The third source of sensitivity to non-coherent spectral components in the input channel is due to distortion that is generated at the output of the multiplier. This effect can also be modelled as a separate functional block, as is shown in Fig. 6.21.

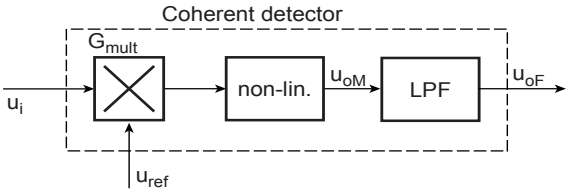

Figure 6.21, Modelling the non-linear distortion at the output of the multiplier.

When considering this effect only (i.e. assuming no distortion in the input channel or reference channel), the output signal can be expressed as:

$$u_{oM} = G_{mult}\left[\left(u_r \times u_i\right) + \delta_2\left(u_r \times u_i\right)^2 + \delta_3\left(u_r \times u_i\right)^3 + ...\right], \tag{6-28}$$

where δ_i denotes the i^{th}-order distortion generated at the output of the multiplier. Assuming only a second-order distortion yields:

$$\begin{aligned} u_{oM} =& G_{mult}\hat{u}_r\hat{u}_i\left[\left(\cos\left(\omega_r t\right)\times\cos\left(\omega_i t\right)\right) + \delta_2\hat{u}_r\hat{u}_i\left(\cos\left(\omega_r t\right)\times\cos\left(\omega_i t\right)\right)^2\right] = \\ & G_{mult}\frac{\hat{u}_r\hat{u}_i}{2}\left[\cos\left(\left(\omega_r \pm \omega_i\right)t\right) + \frac{\delta_2\hat{u}_r\hat{u}_i}{2}\left(1+\cos\left(2\omega_r t\right)\right)\left(1+\cos\left(2\omega_i t\right)\right)\right] = \\ & G_{mult}\frac{\hat{u}_r\hat{u}_i}{2}\left[\cos\left(\left(\omega_r \pm \omega_i\right)t\right) + \frac{\delta_2\hat{u}_r\hat{u}_i}{2}\times\right. \\ & \left.\left(1+\cos\left(2\omega_r t\right)+\cos\left(2\omega_i t\right)+\frac{1}{2}\left(\cos\left(2\left(\omega_r \pm \omega_i\right)t\right)\right)\right)\right] \end{aligned} \tag{6-29}$$

Low-pass filtering at $\omega_{LPF} \ll \omega_r$ results in the following DC and low-frequency components:

$$u_{oF} = G_{mult}G_{LPF}\frac{\hat{u}_r\hat{u}_i}{2}\left[\cos\left(\left(\omega_r - \omega_i\right)t\right) + \frac{\delta_2\hat{u}_r\hat{u}_i}{2}\left(1+\frac{1}{2}\cos\left(2\left(\omega_r - \omega_i\right)t\right)\right)\right] \tag{6-30}$$

The result is an additional DC component and an additional coherent component, both of which are proportional to the distortion. This effect is observed for all even-order harmonic distortion components at the output of the multiplier.

Note that the amount of distortion in a practical system strongly depends on the amplitude of the signal. The voltage generated at the output of a multiplier that is connected to a power supply voltage level V_s cannot exceed this level. In a well-

designed system the maximum peak-to-peak dynamic range of the output voltage is slightly lower than the supply voltage level. However, the saturation occurring at such a level does generate harmonic distortion. Also the input should usually not be driven beyond the power supply voltage level to avoid distortion. This circumstance has a direct impact on the acceptable gain of the multiplier, G_{mult}. If both inputs are driven to values close to the power supply voltage, this gain should be designed such, that also the output voltage is at V_{s}. Hence, $G_{\text{mult,max}}= 2\hat{u}_{\text{o1}}/(2\hat{u}_{\text{i}}\times 2\hat{u}_{\text{r}})= 1/V_{\text{s}}$ $[\text{V}]^{-1} \ll 1$, with $2\hat{u}_{\text{i,max}}= 2\hat{u}_{\text{r,max}}= 2\hat{u}_{\text{o,max}}= V_{\text{s}}$.

A final source of error is due to offset. Multiplying two DC signals obviously results in a DC component at the output of the multiplier. Therefore, multiplying $u_{\text{i}}= \hat{u}_{\text{i}}\cos(\omega_{\text{i}}t)+ U_{\text{i,os}}$ and $u_{\text{r}}= \hat{u}_{\text{r}}\cos(\omega_{\text{r}}t)+ U_{\text{r,os}}$ yields, after low-pass filtering, an output voltage that is expressed as:

$$U_{oF} = G_{LPF}G_{mult}\left(\frac{\hat{u}_i\hat{u}_r}{2}\cos\left(\left(\omega_i-\omega_r\right)t\right)+U_{i,os}U_{r,os}\right) \tag{6-31}$$

It can be concluded that distortion results in a detection limit relative to the amplitude of the signals at the input channel (Eqn. 6-26) and the reference channel (Eqn. 6-23), whereas offset results in an absolute detection limit.

Example 6.6
The input channel of the synchronous detector shown in Fig. 6.22 is connected to a voltage $U_{\text{i}}(t)= 2\times\sin(\omega t)+0.3\times\sin(2\omega t)+0.2\times\sin(3\omega t)$ [V]. The reference channel is connected to a voltage $U_{\text{r}}(t)= 0.2+ 1\times\sin(\omega t)+ 0.01\times\sin(3\omega t)$ [V]. The transfer function of the analog multiplier is expressed as: $U_{\text{o1}}= G_{\text{mult}}\times U_{\text{i}}\times U_{\text{r}}= U_{\text{i}}\times U_{\text{r}}/10$, with the conversion gain $G_{\text{mult}}=0.1\ \text{V}^{-1}$. The low-pass filter can be assumed ideal with a unity gain in the pass band, $G_{\text{LPF}}=1$, zero gain in the blocking band and a cut-off frequency $\omega_{\text{LPF}} \ll \omega$.

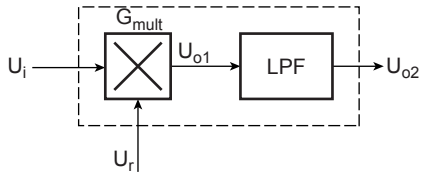

Figure 6.22, Synchronous detector with multi-component signals at the input and reference channel.

1. Calculate for the specified input signal $U_{\text{i}}(t)$, reference signal, $U_{\text{r}}(t)$ and synchronous detector, the output voltage U_{o2} in the case of a synchronous detector with an ideal input channel and reference channel.

2. Similarly, calculate U_{o2} in the case of a non-ideal input channel with an offset voltage $U_{i,os}$= 5 mV and an ideal reference channel.
3. Finally, calculate U_{o2} in the case of a non-ideal input channel with an offset voltage $U_{i,os}$= 5 mV and a non-ideal reference channel with a 10% 2nd harmonic distortion.

Solutions:
1. $U_{o1} = U_i(t)\times U_r(t)/10 = [2\sin(\omega t)+ 0.3\sin(2\omega t)+ 0.2\sin(3\omega t)]\times [0.2 + \sin(\omega t) + 0.01\sin(3\omega t)]/10] =$
$0.4\times\sin(\omega t)/10 + 2[1-\cos(2\omega t)]/20 + 0.02[\cos(2\omega t) - \cos(4\omega t)]/20 +$
$0.06\times\sin(2\omega t)/10+ 0.3[\cos(\omega t)-\cos(3\omega t)]/20+ 0.003[\cos(\omega t)-\cos(5\omega t)]/20+$
$0.04\times\sin(3\ \omega t)/10 + 0.2[\cos(2\omega t)-\cos(4\omega t)]/20 + 0.002[1-\cos(6\omega t)]/20.$

(n.b. $\sin(\alpha)\times\sin(\beta)= [\cos(\alpha-\beta)-\cos(\alpha+\beta)]/2.$)
The DC-terms are selected in the low-pass filter, thus U_{o2}= 2/20+ 0.002/20 = 0.1001 V.

2. The offset in the input channel results in an additional DC term at the output of the multiplier, due to the DC-term in the reference signal: U_{o2}(extra)= 0.005×0.2/10= 0.0001. Total: U_{o2}= 0.1002 V.

3. At the given frequency components in U_r(t), the 2nd harmonic distortion causes additional components at: 2ω and 6ω. The term at 2ω results in a DC-term at the output due to the 2nd harmonic in the signal on the input channel. After multiplication, an extra term equal to: 0.3×10%×(1/20)= 0.0015 V. Thus U_{o2}= 0.1017 V results. The component at 6ω does not match a harmonic in the signal on the input channel and thus has no effect.

6.4.3 Switching detectors and phase detectors

The previous section (6.4.2) explains that the non-linearities in the input channel and the reference channel result in parasitic sensitivities for non-coherent spectral components in the input signal. Since the output voltage of the multiplier is directly proportional to the peak amplitude of the voltage at the reference channel (i.e. $\hat{u}_r$ acts as a gain factor), the detector is usually operated over the maximum possible dynamic range of the reference channel. This mode of operation introduces odd-order harmonic distortion, which limits the performance. The coherent detector is, therefore, especially susceptible to non-linearities in the reference channel.

The limitation is basically the available dynamic range of the analog circuits used for realising the multiplier. Recognising this limitation also provides clues for avoiding this effect. Assume one replaced the analog multiplier for a voltage

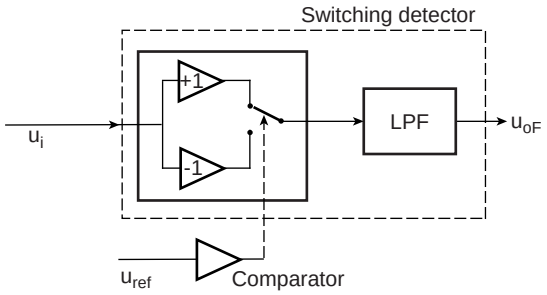

Figure 6.23, Structure of the switching detector.

follower plus an inverting voltage follower that is operated with a switch, as shown in Fig. 6.23. The circuit required for building this **Switching detector** is intrinsically simpler compared to the analog multiplier, and its operation is not limited by the dynamic range of the components. Switching between the inverting and non-inverting voltage follower, is equivalent to analog multiplication of the input signal with a square wave voltage at the reference channel. This does introduce sensitivity to many odd-order harmonics. However, the transfer function no longer depends on $\hat{u}_r$. Therefore, depending on the application, this may not be a serious disadvantage.

Switching between an inverting and non-inverting voltage follower is equivalent to multiplication with a square wave voltage with the Fourier series expressed as: $S(t)=(4/\pi)\ \{\cos(\omega_r t)- 1/3\ \cos(3\omega_r t)+ 1/5\ \cos(5\omega_r t)- 1/7\ \cos(7\omega_r t)...\}$. The output signal of the switching detector results in the case of an input signal $u_i= \hat{u}_i\cos(\omega_i t+\varphi)$ and a frequency synchronous operation ($\omega_i= \omega_r= \omega$) in:

$$\begin{aligned} U_{oM} &= \hat{u}_i \cos(\omega t+\varphi)\left[S(t)\right]= \\ &\hat{u}_i \cos(\omega t+\varphi)\left(\frac{4}{\pi}\left(\cos(\omega t)-\frac{\cos(3\omega t)}{3}+\frac{\cos(5\omega t)}{5}-...\right)\right)= \\ &\frac{2\hat{u}_i}{\pi}\left(\cos(\varphi)+\cos(2\omega t+\varphi)+\frac{\cos(2\omega t+\varphi)}{3}+\frac{\cos(4\omega t+\varphi)}{3}+...\right) \end{aligned} \tag{6-32}$$

Low-pass filtering at $\omega_{LPF} \ll \omega$ results in:

$$U_{oF}=\frac{2\hat{u}_i}{\pi}\cos(\theta) \tag{6-33}$$

Therefore, the basic transfer function of the switching detector is similar to that of the coherent detector with non-linearity in the reference channel (Eqn. 6-22). The increased sensitivity to unwanted spectral components should be reflected in the Signal-to-Noise Ratio, SNR.

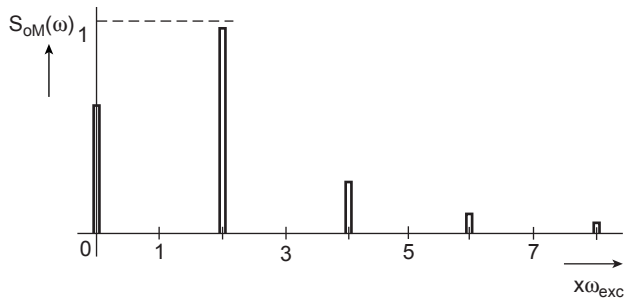

Figure 6.24, Spectrum at the output of the switching detector as a function of ω_{exc} for $\hat{u}_i$= 1V and

Figure 6.24 shows the spectral distribution of the baseband signal and harmonics at the output of the switching detector after low-pass filtering. The noise content in the signal at the input channel in the passband at 3ω, 5ω, 7ω, etc., gives rise to LF noise at the output. These components are within the passband of the LPF and, therefore, contribute to the output signal of the switching detector. The noise within the passband at ω is equal to: $N_o \times 2f_{LPF}$, with N_o as the noise spectral power. Therefore, the total noise at the output of the coherent detector is equal to: $N_o \times 2f_{LPF}$. The Fourier series of a square wave voltage can be used to derive an expression for the total noise at the output of the switching detector:

$$u_{n,SD}^2 = N_o \times 2f_{LPF} + \frac{N_o \times 2f_{LDF}}{3^2} + \frac{N_o \times 2f_{LDF}}{(-5)^2} + \frac{N_o \times 2f_{LDF}}{7^2} + ... =$$
$$N_o \times 2f_{LDF}\left[1 + \left(\frac{1}{3}\right)^2 + \left(\frac{1}{5}\right)^2 + \left(\frac{1}{7}\right)^2 + ...\right] = N_o \times 2f_{LDF}\sum_{n=0}^{\infty}\left(\frac{1}{2n+1}\right)^2 = \frac{\pi^2}{8} N_o \times 2f_{LDF} \quad (6\text{-}34)$$

The noise performance of the switching detector reduces by a factor of $\pi^2/8$= 0.9 dB, which is very acceptable for a wide range of applications.

The phase transfer function of both the coherent detector and switching detector is a (co)sine. Implementing a comparator in the input channel can remove the amplitude information from the input voltage, which results in a linear phase transfer function. This **phase detector** is shown in Fig. 6.25. Since two square wave voltages with a fixed-value peak amplitude are multiplied, the multiplier can be implemented as a logical function (the exclusive OR gate). The obvious disadvantage is the sensitivity to sub- and super-harmonic components in the input signal. The main application of the phase detector is in a **Phase Locked Loop (PLL)**, which is shown schematically in Fig. 6.26.

A **voltage-controlled oscillator (VCO)** is used, which generates an output signal of constant amplitude and a frequency proportional to a control voltage, ω_o=

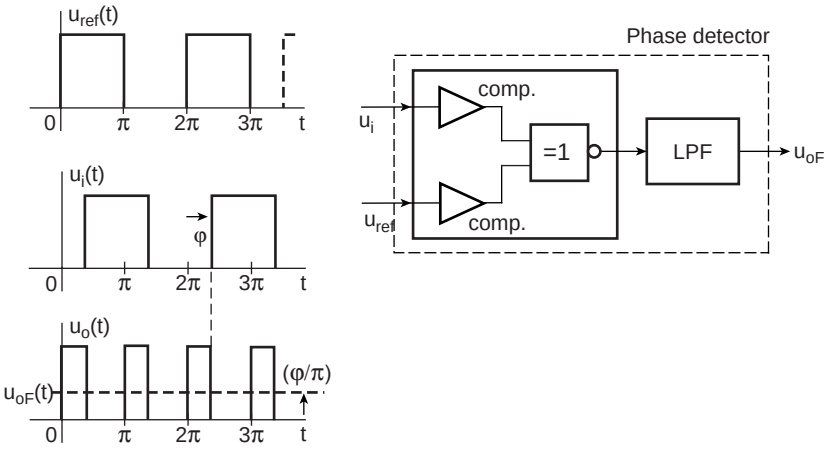

Figure 6.25, Structure of the phase detector.

$K_{VCO} \times U_{oF}$, with K_{VCO} the VCO transfer function [Hz/V]. The phase detector controls the VCO in such a way, using the LPF and an amplifier, that a stationary situation is reached with $\omega_o = \omega_i$ (the excitation signal is captured and the system 'locks'). The coherent frequency becomes available and cleared from variations in the input signal of frequency $\omega > \omega_{LPF}$, such as noise. The PLL is able to track variations in ω_i within its 'holding range'. The critical component is the LPF, which should be designed to remove noise, but also to track changes in the excitation frequency. The quality of the VCO is specified in terms of its locking range and tracking range.

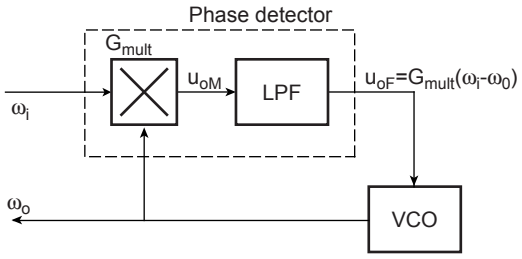

Figure 6.26, Using the phase detector in a PLL to recover the excitation frequency from the input signal.

In applications such as AC-operated Wheatstone bridge read-out, the excitation signal is physically available and can be directly connected to the reference channel. In non-localised wireless-operated systems this is not the case. Therefore, the excitation signal has to be retrieved from the input channel of the coherent detector. The sensor output signal is at this channel, which contains the bridge excitation frequency. The bridge excitation frequency can be retrieved from the composite signal using a PLL, as is shown in Fig. 6.26.

6.4.4 Lock-in amplifier

The use of the terms *coherent* and *synchronous* sometimes leads to confusion. The name of the general technique is **coherent detection**. The multiplier/low-pass filter combination is referred to as the **synchronous detector**.

Two signals are considered coherent when their frequency is the same (the signals are synchronous) and the phase difference is zero.

The synchronous frequency is in principle a sufficient condition for the ideal coherent detector to supply a constant output signal that is proportional to the amplitude of the input signals. However, in the case of a phase difference φ , a multiplicative correction term $\cos(\varphi)$ should be applied (see Eqn. 6-21). Therefore, an unknown phase difference complicates the amplitude measurement. However in the case of well-determined amplitudes, a phase measurement is possible.

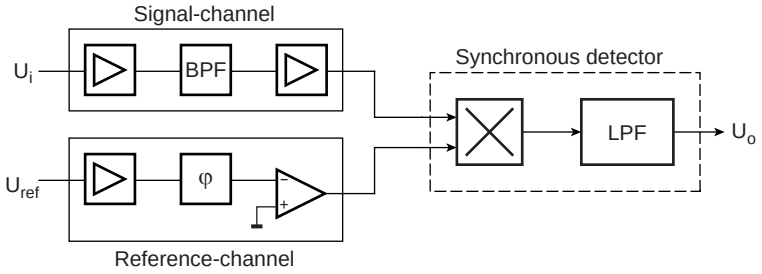

Figure 6.27, Simplified diagram of the lock-in amplifier.

A professional instrument that is based on the coherent detector, but in addition is equipped with analog signal conditioning facilities, is the **lock-in amplifier**. The simplified structural diagram is shown in Fig. 6.27. The lock-in amplifier contains two input channels -the **signal channel** and the **reference channel**- plus the synchronous detector. The signal channel is composed of gain sections and a bandpass filter. The filter is intended to remove some of the wide-band input noise.

The gain section in the input channel and minimizing noise before synchronous detection makes it possible to have a maximum signal level at the multiplier input without saturating the multiplier with wide-band noise. Since saturation leads to the non-linear distortion discussed above, such a measure maximises the overall performance. The reference channel is equipped with a variable phase network that can be used to compensate for a phase change between the synchronous frequencies at the input channel and reference channel. Basically, this facil-

ity makes it possible for the user to tune $\cos(\varphi_{ext} - \varphi_{int}) = 1$, so that maximum sensitivity is achieved.

Note that a non-coherent frequency component of high amplitude does not result in an output signal, but may nevertheless give rise to saturation of the amplifiers in the signal channel or the input of the multiplier. This can easily occur in the case of a narrowband signal of small amplitude contained within a relatively wideband noise of high amplitude. In principle the dynamic range of the system is exceeded at the input of the multiplier without the user noticing. The lock-in amplifier is for that reason usually equipped with a facility to generate a warning in case one of the inputs of the multiplier exceeds the dynamic range by driving an indicator or sending an error code. A Voltmeter is used to display the measurement result.

Example 6.7
Figure 6.28 shows the front panel of a lock-in amplifier. On the lower-left side are the connectors for the differential input of the input channel and the settings of the pre-detection filter. Also on the left-hand side of the instrument are arrow keys for selecting the sensitivity, which can be set between a 1 nV and 1V full scale. The instrument is equipped with two synchronous detectors, channel 1 and channel 2, which enables the simultaneous measurement of both the in-phase component (real part of the transfer from excitation source to input channel) and quadrature component (90^o out of phase= imaginary part) of the signal on the input channel.

Figure 6.28, Front panel of a lock-in amplifier.

The push buttons underneath the display are used to control several instrument functions, such as the cut-off frequency of the low-pass filter, AC-gain in the input channel, DC-gain in the low-pass filter, etc. On the right-hand side of the instrument is the reference channel with its controls and a local oscillator that can be used as the excitation source.

The performance of the lock-in amplifier is mainly determined by the multiplier. Fast AD converters and **Digital Signal Processors (DSPs)** can be used to replace the analog multiplier, as shown in Fig. 6.29. Efficient algorithms are available for digital multiplication. In principle the sampled and quantised input signal is multiplied with the values in a sine and cosine look-up table. The differential frequency is used to drive a PLL, which synchronises the DSP clock frequency, to the frequency at the reference channel. Digital frequency synthesis enables a stable and accurate phase setting. The performance is generally better as compared to the analog version. However, the frequency range is restricted by the DSP.

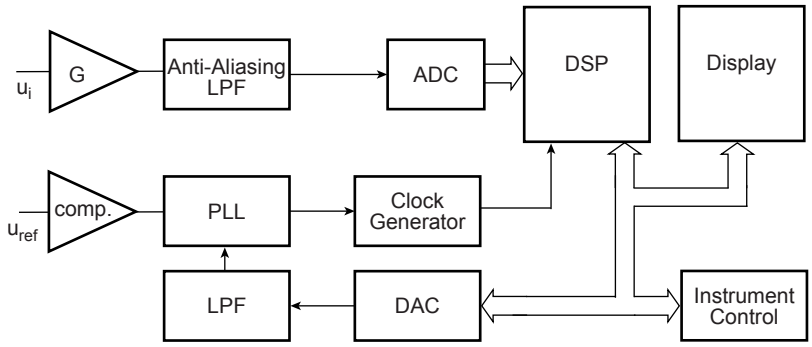

Figure 6.29, Digital lock-in amplifier.

Example 6.8
The reduction in the detection limit that can be achieved when using coherent detection for sensor read-out can be demonstrated in the differential capacitive transducer shown in Fig. 6.30.

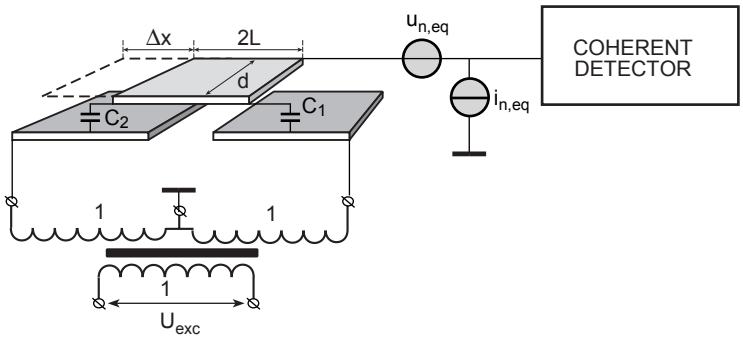

Figure 6.30, Using coherent detection for capacitive sensor read-out.

For $C_1 = C_o - \Delta C$ and $C_2 = C_o + \Delta C$ the sensitivity of this system to changes in capacitance is equal to:

$$\frac{U_o}{U_{exc}} = \frac{(j\omega C_1)^{-1}}{(j\omega C_1)^{-1}+(j\omega C_1)^{-1}} - \frac{(j\omega C_2)^{-1}}{(j\omega C_1)^{-1}+(j\omega C_1)^{-1}} = \frac{C_2 - C_1}{C_2 + C_1} = \frac{\Delta C}{C_o}$$
$$\rightarrow S_C^{Uo} = \frac{U_{exc}}{C_o} \tag{6-35}$$

The output impedance of the differential capacitive transducer is determined by C_1 in parallel to C_2: $Z = (j\omega 2C_o)^{-1}$. Therefore, the effect of the input-referred spectral noise power amounts to:

$$s_{n,i} = s_{n,u_{eq}} + \frac{s_{n,i_{eq}}}{4\omega^2 C_o^2}\left[V^2/Hz\right] \tag{6-36}$$

Capacitive measurements are preferably done at high frequencies, hence in good approximation $N_o = u_{n,eq}^2$. When only considering the coherent noise with the bandwidth of the low-pass filter, the total noise at the input is equal to:

$$u_{n,i}^2 = 2 f_{LPF} s_{n,i} \ [\mathrm{V}^2] \tag{6-37}$$

An excitation voltage with an rms-value $u_{exc} = 5$ V, a nominal transducer capacitance $C_o = 100$ pF, a noise bandwidth at 1 Hz and an input-referred noise voltage at 10 nV/√Hz results in a detection limit at:

$$\Delta C^2 = \left(\frac{C_o}{u_{exc}}\right)^2 u_{n,i}^2 = 4\times 10^{-22} \times 2 \times 10^{-16} = 8 \times 10^{-38}\ F^2$$
$$\rightarrow \Delta C_{\mathrm{det}} = 0.29\,\mathrm{aF} \tag{6-38}$$

Other effects, such as temperature dependence and the humidity dependence of the capacitance, usually become limiting at such an extremely low detection limit.

6.5 Correlation

The **cross correlation** between two stochastic signals $x(t)$ and $y(t)$ is defined as:

$$R_{xy}(\tau) = \lim_{T\to\infty} \frac{1}{T} \int_{-T/2}^{T/2} x(t)\cdot y(t+\tau)dt \tag{6-39}$$

The cross-correlation indicates the level of matching between two time series to be a function of a variable delay time between them. If the stochastic signal y(t) originates from $x(t)$, yet delayed over t', then $R_{xy}(\tau)$ is maximum for $\tau = t'$. The **Auto-correlation** is a special case in which the matching of this signal with

itself after a variable delay time is calculated. The maximum value of the auto-correlation function is at $\tau = 0$.

Correlation is a very suitable technique for measuring a quantity that is somehow encoded in the delay of a noisy signal. Examples of applications that are discussed in this section are:

- Thermal flow velocity measurement in fluids
- Acoustic leak detection

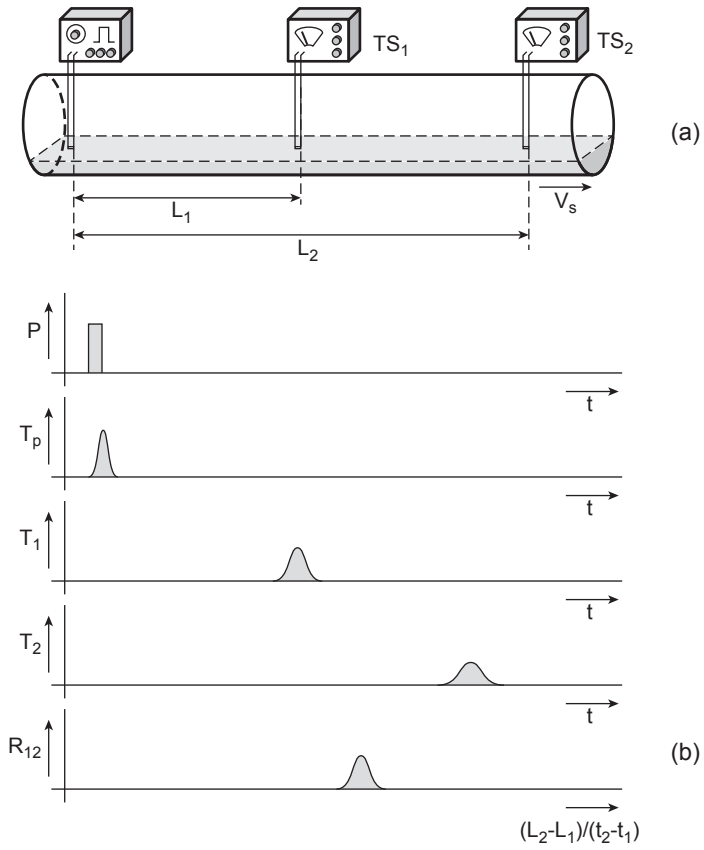

Figure 6.31, (a) Flow measurement in a fluid based on correlation of the output signals of the temperature sensors and (b) a typical measurement cycle.

In the thermal flow velocity measurement system that is shown in Fig. 6.31, a heat pulse is locally generated. The heat pulse is propagated through the fluid by two mechanisms. The first is the fluid flow, which basically carries the heated sample of liquid along with the general flow. The second is due to diffusion of the heat contained within the heated sample. In thermal equilibrium, the heat is

redistributed throughout the fluid, so that a uniform temperature is reached. Operation of the flow velocity measurement system is also shown in Fig. 6.31.

A current pulse applied to a heating element (a resistor) generates a heat pulse, which propagates through the fluid and, after a certain time t_1, the heated sample reaches a temperature sensor TS_1 which is located a distance L_1 downstream from the heating element. The time interval between the generation and detection of the thermal peak is equal to: $t_1 = L_1/v_{flow}$, which enables a direct measurement of v_{flow}.

The first problem in this system is that the heat capacitance of the heating element causes the temperature peak at the moment of generation to be delayed with respect to the timing of the current pulse, thus yielding a significant measurement uncertainty. This problem is solved by adding a second temperature sensor, TS_2, at a distance L_2 from the heating element. The time difference, $\Delta t = t_2 - t_1$ satisfies the relation: $\Delta t = (L_2 - L_1)/v_{flow}$, thus $v_{flow} = (L_2 - L_1)/(t_2 - t_1)$.

The second problem is the influence of diffusion. As diffusion removes heat omni-directionally and away from the hot spot, it does not affect the position of maximum temperature, while the heated sample moves along the temperature sensors. However, diffusion does lower the maximum temperature, as the heat becomes distributed over time and causes broadening of the pulse, as is shown in Fig. 6.31b. This effect complicates the measurement of the moment that the heat pulse has its maximum value after propagation over distances L_1 and L_2. Correlation can conveniently be used to solve this measurement problem. The signals of the two temperature sensors are used as the input of the correlator, while the maximum of the correlogram is at $R_{TS1/TS2}(t_2 - t_1)$ and determines v_{flow}.

Another application of the correlator is in leak detection based on the measurement of a relative delay time that is due to the propagation of sound along different lengths of a tube. Assume a tube transporting a fluid, as shown in Fig. 6.32, with two microphones connected to the outside of the tube wall at well-defined positions A and B. If there is a leak in the wall of the tube, some fluid leaks out, which generates an acoustic signal. This acoustic signal propagates along the wall of the tube in both directions and reaches the two microphones. The location of the leak can be determined from the difference in delay time. As the source of both acoustic signals reaching a microphone is a random signal originating from the same leak, a correlator can be used to measure the differential delay time: $\Delta t = (L_2 - L_1)/v_{acous}$.

Rather than digging a long trench, the leak can be detected by digging access holes at fixed intervals along the tube at which microphones are placed. Of

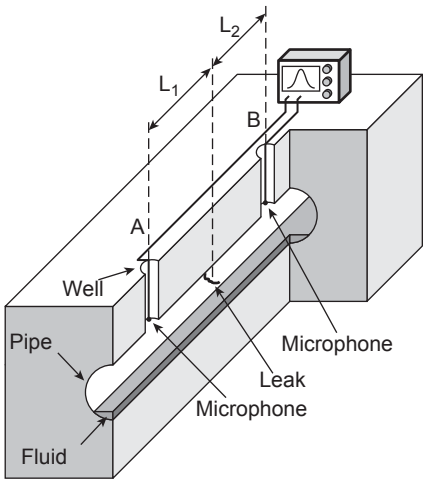

Figure 6.32, Leak detection based on the correlation of output signals of two microphones.

course, there are many sources of acoustic noise within the tube. Most are randomly generated at positions along the tube wall that change in time and do not show up in the correlogram. However, any irregularity in the tube geometry that results in an acoustic signal caused by the flow through it, results in a peak in the correlogram.

The propagation velocity in a steel tube is about 5000 m/s. Therefore, a leak one metre from the centre between locations A and B results in a differential delay time: t_1-t_2= 0.4 ms (note that L_2-L_1= 1-(-1)= 2 metres). This is well within the range of state-of-the-art correlometers.

6.6 Digital system control for improved detectivity

Instruments are usually equipped with a digital system control unit, which can be used to enhance detectivity. The measurement result can be influenced by the digital system control in two ways:

- Off-line by switching (analog) units on and off
- On-line by digital signal processing the measurement data

Off-line digital control of a front-end amplifier can be used to reduce offset significantly. Figure 6.33 shows the basic non-inverting amplifier. However, in this case a switch is included that enables short-circuiting of the input.

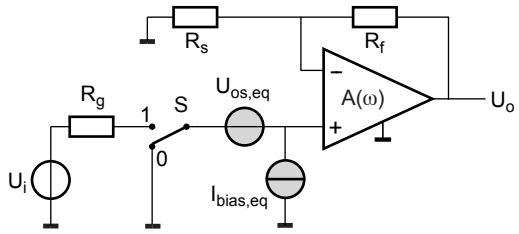

Figure 6.33, Offset correction.

During the measurement phase, ϕ_1, switch S is in position S= 1 and the transfer function is described by: $U_o(\phi_1)= G_v(U_i+ U_{os,eq}+ I_{bias,eq}R_g)$. However, during the zeroing phase, ϕ_0, switch S is in position S= 0 and the transfer function is described by: $U_o(\phi_0)= G_v(U_{os,eq})$. Subtraction results in: $U_o(\phi_1)-U_o(\phi_1)= G_v(U_i+ I_{bias,eq}R_g)$. Therefore, the effect of the equivalent input offset voltage, $U_{os,eq}$, has been eliminated. More sophisticated implementations of this principle can be used to compensate for other non-idealities, such as variations in the full-scale reference or non-linearity. This principle is very suitable to implement in **switched capacitor** circuits.

A more advanced implementation makes use of the fact that a measurement result that is obtained in a setup affected by noise can be represented by a Gaussian distribution with an average value, μ_m, determined by the amplitude of the intended (deterministic) measurement signal and the variance, σ^2, determined by the power of the (stochastic) noise.

The variance is reduced when averaging over several measurements, whereas the average remains unchanged. Averaging over m measurements results in:

$$\mu = \mu_m \ , \ \sigma^2 = \frac{\sigma_m^2}{m} \tag{6-40}$$

The resulting equivalent quantisation noise is expressed as:

$$\begin{aligned} SNR_m &= 10^{10}\log\left(\frac{P_s}{P_n}\right) = 10^{10}\log\left(\frac{\mu^2}{\sigma^2}\right) = 10^{10}\log\left(\frac{\mu_m^2}{\sigma_m^2/m}\right) = \\ &10^{10}\log\left(\frac{\mu_m^2}{\sigma_m^2}\right) + 10^{10}\log(m) = SNR_1 + 10^{10}\log(m)[dB] \end{aligned} \tag{6-41}$$

The first term denotes the SNR of one single measurement and the second term the noise reduction due to averaging. Averaging over m= 4 samples results in a 6 dB improvement (half the noise power).

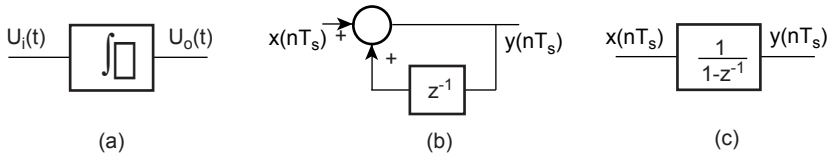

Figure 6.34, Realisation of the summator in (a) the analog domain, (b) the digital domain and (c) equivalent block diagram in the z-domain.

It should be noted that averaging by adding numbers in the digital domain is equivalent to integration in the time-continuous analog domain (Fig. 6.34). Averaging over m measurements basically implies an m-fold measurement time. Integration of a signal over this extended measurement time results in an m^2-fold signal power. The noise power increases m-fold to that of a single measurement. Therefore, the overall effect is an m-fold improved SNR.

Adding four binary numbers results in two additional bits of which only one is significant in terms of SNR (Eqn. 6-41). Therefore, simple averaging is not an efficient technique for reducing quantisation noise. More efficient approaches are available such as **ΣΔ-modulators**, which are not discussed here.

On-line digital signal processing has found widespread application in electronic instrumentation. Many instruments are realised using primarily digital building blocks. An example is the digital lock-in amplifier presented in Fig. 6.29. Other analog functional blocks discussed in this chapter, such as the correlator, have also been replaced with a digital implementation. Finally, correction, as described in Section 6.2.2, is basically on-line digital signal processing. The functionality has not changed, which makes the description in terms of analog functional blocks very useful. Digital signal processing is not discussed here.

6.7 Exercises

Figure 6.14 shows a non-inverting amplifier that is used to read-out a voltage source, u_i. Assume a fixed-value and a well-defined source resistance R_g= 2 kΩ. The specifications of the OPAMP are:

- U_{os}= 0.2 mV and I_{bias}= 1 nA (I_{os}= 0 nA)
- Open-loop gain, $A(\omega)= A_o/(1+j\omega\tau_v)$, with A_o= 94 dB and the unity-gain frequency f_T= 2 MHz
- Open-loop input impedance composed of a resistor R_i= 10 MΩ in parallel to an input capacitance C_i= 1 pF
- Open-loop output resistance R_o= 100 Ω.

6.1 Calculate from the specifications: (a) τ_v and (b) the bandwidth of the non-inverting amplifier for a gain $|G_f| = |u_o/u_i| = 100$.

Solution:

$$\begin{aligned} \tau_v &= \frac{A_o}{\omega_T} = \frac{A_o}{2\pi \times f_T} = \frac{10^5/2}{2\pi \times 2 \times 10^6} = \frac{1}{80\pi} s \\ f_f \times A_f &= f_T \times 1 \rightarrow f_f = f_T / A_f = 20\,kHz \end{aligned} \tag{6-42}$$

6.2 Calculate the input-referred equivalent offset sources for the bias-compensated non-inverting amplifier, as discussed in Chapter 2, and select component values for the gain setting that is indicated in Question 6.1 with bias current compensation.

Solution:

$$\left.\begin{aligned} G_f &= \frac{R_s + R_f}{R_s} = 100 \rightarrow R_f = 99 \times R_s \\ R_g &= \frac{R_s \times R_f}{R_s + R_f} = 2000 \end{aligned}\right\} \rightarrow \frac{R_s \times 99R_s}{R_s + 99R_s} = 2000 \rightarrow \begin{matrix} R_s = 200/99 k\Omega \\ R_f = 200 k\Omega \end{matrix} \tag{6-43}$$

6.3 Calculate the input impedance, Z_{is}, of the non-inverting amplifier at 1 kHz and the resulting overall gain error due to source loading.

Solution:

$$\left.\begin{aligned} Z_{is} &= \frac{\left[A(\omega)+1\right]R_s + R_f}{R_s + R_f} Z_i \\ A\left(\omega \gg \frac{1}{\tau_v}\right) &\approx \frac{A_o}{j\omega\tau_v} = -j\frac{\omega_T}{\omega} \\ Z_i &= \frac{R_i}{1 + j\omega R_i C_i} = \frac{10^7}{1 + j2\pi \times 10^{-2}} \end{aligned}\right\} \rightarrow \begin{matrix} Z_{is} = \left(1 - j\frac{\omega_T}{\omega}\frac{R_s}{R_s + R_f}\right) Z_i = (1 - j20) Z_i \\ Z_{is}(1kHz) = (226 - j2002) 10^5\,\Omega \end{matrix} \tag{6-44}$$

Hence:

$$\varepsilon_1 = \frac{R_g}{R_g + |Z_{is}|} = \frac{2 \times 10^3}{2 \times 10^3 + 2015 \times 10^5} = 10^{-5} \tag{6-45}$$

6.4 Calculate the output impedance, Z_{os}, of the non-inverting amplifier at 1 kHz and the resulting overall gain error due to output loading by a capacitive load C_L= 100 pF.

Solution:

$$Z_{os} \approx R_o \frac{R_s + R_f}{A(\omega) R_s} = R_o \frac{\left(R_s + R_f\right) j\omega}{R_s \omega_T} = j100 \frac{100 \times 2\pi \times 10^3}{2\pi \times 2 \times 10^6} = j5\Omega \rightarrow$$
$$L_{os} = R_o \frac{R_s + R_f}{R_s \omega_T} = 796\,\mu H \;,\; \varepsilon_3 = \frac{|Z_{os}|}{|Z_{os}| + |Z_L|} = \frac{5}{5 + 1.59 \times 10^6} = 3 \times 10^{-6} \quad (6\text{-}46)$$

6.5 Calculate the overall uncertainty of the read-out due to offset and compare this with the uncertainty due to scale error (which is due to the combined effect of source loading and deviation from the nominal transfer function G_f= 100, because of the finite open-loop gain and output loading), for an input amplitude $u_{i,rms}$= 8 mV at 1 kHz.

Solution:

$$\frac{u_o(\omega)}{u_i(\omega)} = \frac{\frac{R_s + R_f}{R_s}\left(1 - \frac{R_s + R_f}{A_o R_s}\right)}{1 + j\omega\tau_v \frac{R_s + R_f}{A_o R_s}} = G_f\left(1 - \varepsilon_2\right) \rightarrow \varepsilon_2\left(1kHz\right) = 3.2 \times 10^{-3} \quad (6\text{-}47)$$

The (relative) error in the nominal transfer function is much larger than that due to loading errors. The (absolute) error for an 8 mV input signal is equal to: $3.2\times10^{-3}\times8\times10^{-3}$= 25.6 μV. Since the bias currents are compensated for, the equivalent input offset voltage is equal to U_{os}= 200 μV, which is much larger.

The coherent detector shown in Fig. 6.22 has a conversion gain of G_{mult}=0.1 V^{-1}. The cut-off frequency of the low-pass filter is at a frequency much lower than the baseband signal at the input or reference channel, $\omega_c \ll min\{\omega_i, \omega_r\}$. For problems 6.6-6.8 assume the signal at the input channel is described by:

$U_i(\omega)$= 0.002+ $y\times\cos(\omega_i t)$+0.01×$\cos(2\omega_i t)$ [V] and at the reference channel by: $U_r(\omega)$= 1×$\cos(\omega_r t)$+ $a_2\times\cos(2\omega_i t)$+ $a_3\times\cos(3\omega_i t)$ [V].

6.6 Calculate the maximum acceptable offset in the reference channel, U_{os}, for a detection limit at y = 100 nV (assume for this question $\omega_i = \omega_r$ and $a_2 = a_3$= 0).

Solution:

$$U_{o,LPF}(OS) \le U_{o,LPF}(y) \rightarrow G_{mult} \times U_{os,i} \times U_{os,r} \le \frac{G_{mult}}{2} \times 1 \times y \rightarrow$$
$$U_{os,r} \le \frac{y/2}{U_{os,i}} = \frac{5 \times 10^{-8}}{2 \times 10^{-3}} = 25\,\mu V \tag{6-48}$$

6.7 Calculate the maximum acceptable 2nd harmonic component, a_2, of the reference signal for a detection limit at y = 100 nV (assume for this question $\omega_i = \omega_r$ and $U_{os} = a_3 = 0$).

Solution:

$$U_{o,LPF}(2\omega_r) \le U_{o,LPF}(y) \rightarrow \frac{G_{mult}}{2} \times 0.01 \times a_2 \le \frac{G_{mult}}{2} \times 1 \times y_{\min} \rightarrow$$
$$a_2 \le \frac{y_{\min}}{0.01} = \frac{10^{-7}}{10^{-2}} = 10\,\mu V \tag{6-49}$$

6.8 Calculate the maximum acceptable 3rd harmonic component, a_3, of the reference signal for a detection limit at y = 100 nV (assume for this question $\omega_i = \omega_r$ and $U_{os} = a_2 = 0$).

Solution:

$$U_{o,LPF}(3\omega_r) \le U_{o,LPF}(y) \rightarrow \frac{G_{mult}}{2} \times 0 \times a_3 \le \frac{G_{mult}}{2} \times 1 \times y_{\min} \rightarrow a_3 \le \frac{y_{\min}}{0} \tag{6-50}$$

Note that the 3*rd* harmonic is not present in the input signal. Therefore, a_3 is not limited.

The next question assumes a sinewave voltage of coherent frequency, $\omega_r = \omega_r$, but unknown peak amplitude, $\hat{u}_r = \hat{u}_i$, at the input and the reference channel: $u_i(\omega) = \hat{u}_i \times \cos(\omega_r t)$ and $u_r(\omega) = \hat{u}_r \times \cos(\omega_r t)$. The positive power supply voltage V_{DD} = +6 V and the negative power supply voltage is at V_{SS} = -6 V. Assume the coherent detector will be fully driven within the range of the power supply voltages and the output can drive to any voltage level within the power supply range without saturation.

6.9 Calculate: (a) the maximum value of $\hat{u}_\mathrm{i}$ and $\hat{u}_\mathrm{r}$ that can be processed in the multiplier and (b) the maximum acceptable conversion gain, $G_\mathrm{mult,max}$.

Solution:

$$\begin{aligned}
&\text{Any input: } 2\hat{u} \le V_\mathrm{dd} - V_\mathrm{ss} \rightarrow \hat{u}_\mathrm{i,max} = \hat{u}_\mathrm{r,max} = 6V \\
&U_\mathrm{o,max} = \frac{G_\mathrm{mult}}{2} \times \hat{u}_\mathrm{i,max} \times \hat{u}_\mathrm{r,max} \left(1 - \cos\left(2\omega_r t\right)\right)_\mathrm{max} \le \frac{V_{dd} - V_{ss}}{2} \rightarrow \\
&G_\mathrm{mult,max} = \frac{\left(V_{dd} - V_{ss}\right)/2}{\left(\hat{u}_\mathrm{i,max} \times \hat{u}_\mathrm{r,max}\right)/2} = \frac{12/2}{6 \times 6/2} = \frac{1}{3} V^{-1}
\end{aligned} \tag{6-51}$$

An instrument for measuring harmonic distortion in a signal is shown simplified in Fig. 6.35. A Phase-Locked Loop (PLL) is used to generate the selected harmonic, n. In the figure the instrument is set to measure the third harmonic content (n= 3) with $\hat{u}_\mathrm{r}$= 1V. A coherent detector with a conversion gain of G_mult= 0.1 V^{-1} and a low-pass filter with a cut-off frequency at a value much smaller than the baseband frequency in the input and unity-gain DC transfer function, are used to measure the signal content in the selected harmonic.

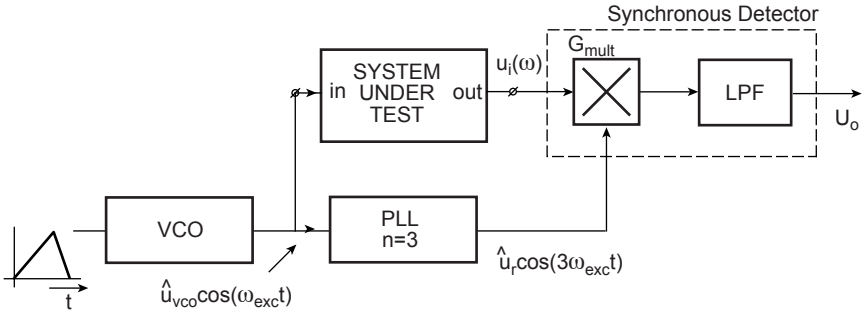

Figure 6.35, Simplified schematic diagram of an instrument for distortion measurement.

The signal at the input channel (i.e. at the output of the system under test) is described by: $U_\mathrm{i}(\omega)$=0.02+ 0.5×cos($\omega_\mathrm{exc}t$)+0.01×cos($2\omega_\mathrm{exc}t$)+0.04×cos($3\omega_\mathrm{exc}t$)+ 0.005×cos($5\omega_\mathrm{exc}t$)+ 8×10^{-4}×cos($7\omega_\mathrm{exc}t$)+ 2×10^{-5}×cos($9\omega_\mathrm{exc}t$) [V].

6.10 Calculate the voltage at the output of the low-pass filter for an ideal coherent detector with a distortion-free signal at the reference channel input.

Solution:

$$U_{o,LPF} = G_{mult} \times \hat{u}_i(3\omega_{exc}) \times \hat{u}_r(3\omega_{exc})/2 = 0.1 \times 0.04 \times 1/2 = 2\,mV \qquad (6\text{-}52)$$

6.11 Calculate the maximum acceptable offset in the reference channel, $U_{os,r}$, for an inaccuracy specification ε= 5% for the measurement of the third harmonic in the input signal (due to this effect only).

Solution:

$$U_{o,LPF} = G_{mult}U_{os,i}U_{os,r} \le \varepsilon \times 2\,mV \rightarrow$$
$$U_{os,r} \le \frac{\varepsilon \times 2\,mV}{G_{mult}U_{os2}} = \frac{5 \times 10^{-2} \times 2 \times 10^{-3}}{0.1 \times 2 \times 10^{-2}} = 50\,mV \qquad (6\text{-}53)$$

6.12 Calculate the required suppression of the baseband frequency in the PLL for the measurement of the third harmonic in the input signal with an inaccuracy specification ε= 5% (due to this effect only).

Solution:

$$G_{mult}\hat{u}_i(\omega_{exc}) \times \hat{u}_r(\omega_{exc})/2 =$$
$$G_{mult}\hat{u}_i(\omega_{exc}) \times \delta_b \times \hat{u}_r(3\omega_{exc})/2 \le \varepsilon \times G_{mult}\hat{u}_i(3\omega_{exc}) \times \hat{u}_r(3\omega_{exc})/2 \rightarrow \qquad (6\text{-}54)$$
$$\delta_{b,\max} = \frac{\varepsilon \times \hat{u}_i(3\omega_{exc})}{\hat{u}_i(\omega_{exc})} = \frac{5 \times 10^{-2} \times 4 \times 10^{-2}}{0.5} = 4 \times 10^{-3}$$

6.13 Calculate the maximum acceptable 2nd harmonic distortion in the reference channel, δ_2, for an inaccuracy specification ε= 5% for the measurement of the third harmonic in the input signal (due to this effect only).

Solution:
A 6th harmonic component is generated in the reference channel. Since $6\omega_{exc}$ is not available in the signal at the input channel, the system is not sensitive to the distortion: δ_2 unlimited.

6.14 Calculate the maximum acceptable 3rd harmonic distortion in the reference channel, δ_3, for an inaccuracy specification ε= 5% for the measurement of the third harmonic in the input signal (due to this effect only).

Solution:
A 9th harmonic component is generated in the reference channel:

$$\begin{aligned} &G_{mult}\hat{u}_i(9\omega_{exc})\times\hat{u}_r(9\omega_{exc})/2 = \\ &\quad G_{mult}\hat{u}_i(9\omega_{exc})\times\delta_3\times\hat{u}_r(3\omega_{exc})/2 \le \varepsilon\times G_{mult}\hat{u}_i(3\omega_{exc})\times\hat{u}_r(3\omega_{exc})/2 \rightarrow \\ &\delta_{3,\max} = \frac{\varepsilon\times\hat{u}_i(3\omega_{exc})}{\hat{u}_i(9\omega_{exc})} = \frac{5\times10^{-2}\times4\times10^{-2}}{2\times10^{-5}} = 10^2 \end{aligned} \tag{6-55}$$

The low sensitivity for the 3rd harmonic component is due to the very low value of $9\omega_{exc}$.